THE ASTROPHYSICAL JOURNAL, 506:384–404, 1998 October 10
© 1998. The American Astronomical Society. All rights reserved. Printed in U.S.A.

THE PISTOL STAR

DONALD F. FIGER,[1] FRANCISCO NAJARRO,[2,3] MARK MORRIS,[1] IAN S. MCLEAN,[1] THOMAS R. GEBALLE,[4]
ANDREA M. GHEZ,[1] AND NORBERT LANGER[5]
Received 1998 February 9; accepted 1998 May 11

ABSTRACT

We present new near-infrared data and analysis, which indicate that the Pistol Star is one of the most luminous stars known, adding another test point for massive star formation and stellar evolution theories. We estimate an extinction of $A_K = 3.2 \pm 0.5$ using the near-infrared colors of the star and of surrounding stars in the young Quintuplet cluster. Using our wind/atmosphere code, we find two families of models that fit the spectral energy distribution and detailed line profiles. The lower luminosity models give $L = 10^{6.6 \pm 0.2}\ L_\odot$ and $T_{\rm eff} = 10^{4.15 \pm 0.01}$ K, while the higher luminosity models give $L = 10^{7.2 \pm 0.2}\ L_\odot$ and $T_{\rm eff} = 10^{4.33 \pm 0.01}$ K; the error in luminosity assumes an uncertainty of ± 0.5 in A_K, while the error in $T_{\rm eff}$ is constrained by detailed line modeling. The models also reveal a helium enriched surface. As previously existing stellar evolution models do not extend to such high luminosities, we employ new evolutionary tracks for very massive stars to determine the initial mass and age of the Pistol Star, and estimate $M_{\rm initial} = 200$–$250\ M_\odot$ and an age of 1.7–2.1 Myr. The inferred luminosity and temperature place the star in a sparsely populated zone in the H-R diagram where luminous blue variables (LBVs) are often found. This is consistent with our evolutionary models, which predict that the star is in an unstable evolutionary stage. We interpret the star and its surrounding nebula as an LBV that has recently ejected large amounts of material. Our K-band speckle-imaging data reveal the star to be single down to a projected separation of 110 AU.

Subject headings: infrared: stars — ISM: individual (G0.15−0.05) — stars: emission-line, Be — stars: evolution — stars: fundamental parameters — supergiants

1. INTRODUCTION

The most massive stars provide limits for star formation and stellar evolution theories. They define the upper mass cutoff for initial mass functions (IMFs) in young clusters. Their luminosities are near the Eddington limit, resulting in prodigious winds and evolutionary trajectories determined by mass loss (Chiosi & Maeder 1986). The metallicities of their natal environments might be important factors in determining their initial masses and the strengths of their winds, and thus their evolutionary progressions.

Some of the most massive stars are variable and eject large amounts of matter in giant eruptions. These luminous blue variables (LBVs) are often regarded as the evolutionary links between main-sequence O stars and the evolved Wolf-Rayet stars. Although they define an important evolutionary stage, only a dozen are known in the local group of galaxies, so the duration of this stage is presumably very short ($< 10^5$ yr).

The Pistol Star is a candidate for the most luminous star known, and given its evolutionary stage, it may have been the most massive when it formed. Located near the Galactic center, it may offer a unique perspective on the evolution of a massive star formed in a high-metallicity environment. The Pistol Star is an LBV, as evidenced by its location in the H-R diagram, its spectral variability, and its surrounding ejecta, which forms the H II region G0.15−0.05 (hereafter, the "Pistol Nebula"; Yusef-Zadeh & Morris 1987).

The Pistol Star is located at the center of curvature of the Pistol Nebula. Its coordinates are R.A. $17^{\rm h}43^{\rm m}4^{\rm s}.8$, decl. $-28°48'57''$ (B1950) according to Nagata et al. (1993), who reported *JHKLMN* photometry for the star (their object No. 25). It appears to be a member of the young Quintuplet cluster (AFGL 2004), located 30 pc, in projection, from the Galactic center (Glass, Catchpole, & Whitelock 1987; Nagata et al. 1990; Okuda et al. 1990; Glass, Moneti, & Moorwood 1990). Figer, Morris, & McLean (1996; hereafter FMM96) identified more than 30 post–main-sequence stars in the cluster having $M_{\rm initial} > 20\ M_\odot$ (the Pistol Star is No. 134 in their list).

Moneti, Glass, & Moorwood (1994) first obtained a low-resolution K-band spectrum of the star (their "serendipitous source"), revealing a strong Brackett-γ emission line. Figer, McLean, & Morris (1995; hereafter FMM95) obtained a similar spectrum ($R \approx 525$; their "star 3"), identified many other emission lines, and estimated $L \approx 10^{6.3}\ L_\odot$. They suggested that this star be considered a luminous blue variable candidate (LBVc) based upon its luminosity, its LBV-like K-band spectrum, and its spatial relationship to the surrounding Pistol Nebula.

Cotera et al. (1996) also estimated a very high luminosity for this star (their "Pistol source A"), $L \approx 10^{7.0}\ L_\odot$, and gave a spectral classification of B[e] based upon K-band spectral morphology. Timmermann et al. (1996) presented a moderate-resolution ($R \approx 1300$) K-band spectrum for it, confirming the weaker lines identified in FMM95. Morris et al. (1996) preferred a B[e] classification for the star based upon their collection of near-infrared spectra of stars that

[1] University of California, Los Angeles, Division of Astronomy, Department of Physics & Astronomy, Los Angeles, CA 90095-1562; figer@astro.ucla.edu.
[2] Institut für Astronomie und Astrophysik der Universität München, Scheinerstrasse-81679 München, Germany.
[3] CSIC, Instituto de Estructura de la Materia, Departamento Molecular Serrano 121, 28006 Madrid, Spain.
[4] Joint Astronomy Centre, 660 N A'ohoku Place, University Park, Hilo, HI 96720.
[5] Institut für Theoretische Physik und Astrophysik, Am Neuen Palais 10, D-14469 Potsdam, Germany.

are thought to be in an intermediate stage of evolution between the main sequence and the WR stages. FMM95, Cotera et al. (1996), Timmermann et al. (1996), and Lang, Goss, & Wood (1997) all suggested that the star may be photoionizing the surrounding Pistol Nebula; FMM95 (also see Figer 1995) suggested further that the Pistol Nebula gas is ejecta from the star.

In this paper, we present new observations of the Pistol Star and its surrounding nebula. The observations and data reduction are discussed in § 2. We use images to obtain JHK'nbL photometryfor the star. We present near-infrared spectra of the star and the nebula in § 3: JHK at low resolution, near–Paschen-α and Brackett-γ at moderate resolution, and near–Brackett-α at high resolution. The spectra and photometry of the star are used to constrain physical parameters, i.e., luminosity and temperature, in wind/atmosphere models in § 4. In § 5, we use our new stellar evolutionary tracks to infer an initial mass and age for the star; we then compare the luminosity and mass to those of other luminous stars. We interpret the Pistol Nebula as circumstellar ejecta from the Pistol Star in § 6. Finally, the conclusions are presented in § 7.

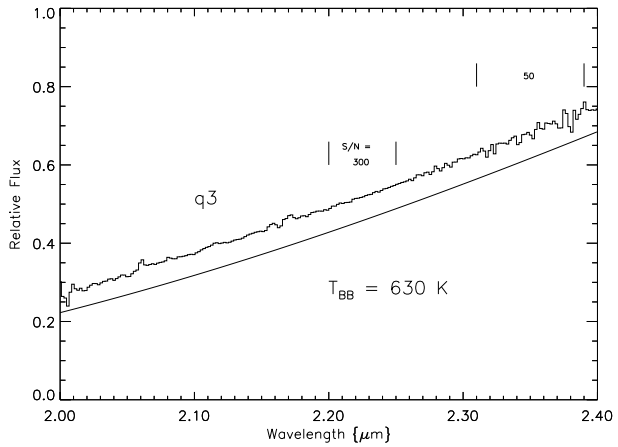

FIG. 1.—Apparent K-band spectrum of q3. A blackbody curve, having $T = 630$ K, has been plotted as a solid line. The features near 2.058 μm and beyond 2.25 μm are due to imperfect atmospheric correction. The feature near 2.166 μm is due to imperfect removal of the Brackett-γ absorption line in the atmospheric standard. The broad hump near 2.11 μm may be intrinsic to the star. The formal signal-to-noise ratio, after dividing by a fit to the continuum, has been labeled for selected wavelength regions in all figures. This spectrum has not been dereddened; however, the remaining spectra have all been dereddened according to the discussion in the text.

2. OBSERVATIONS AND DATA REDUCTION

A summary of all observations is given in Table 1. A more detailed description of the instrumentation and data reduction is given below.

2.1. *Low-Resolution Imaging*

Low-resolution images were obtained with the UCLA double-beam near-infrared camera (McLean et al. 1993, 1994) on the University of California Observatories' 3 m Shane telescope; this combination yields a plate scale of 0.″7 pixel^{-1}. Images were taken in the JHK'nbL filters. In all cases, the telescope was dithered between frames in order to produce a flat field and remove bad pixels in the final images. The "seeing" produced stellar images having $d_{\rm FWHM} \approx 1.''4$. Point-spread function (PSF) fitting routines in IRAF[6] were used to estimate the photometry.

Photometric standards were observed during the night, but because of the relatively large difference in airmass between the target and the standards, the resultant photometry differed by 0.2 mag from the H- and K-band photo-

[6] IRAF is distributed by the National Optical Astronomy Observatories, which are operated by the Association of Universities for Research in Astronomy, Inc., under cooperative agreement with the National Science Foundation.

TABLE 1

SUMMARY OF OBSERVATIONS

Object	Filter/Spectral Range (μm)	Instrument/Telescope/Setup	Date	Integration Time (s)
Pistol Star	J	UCLA[a] /Lick 3 m/imaging	1996 July 4	360
Pistol Star	H	UCLA/Lick 3 m/imaging	1996 July 4	360
Pistol Star	K'	UCLA/Lick 3 m/imaging	1996 July 4	360
Pistol Star	nbL[b]	UCLA/Lick 3 m/imaging	1996 July 4	360
Pistol Star	K	NIRC[c] /Keck I/imaging	1997 July 28	74.5
Pistol Star	H	NIRC[c] /Keck I/imaging	1997 July 28	74.5
Pistol Star	1.139–1.315 (J)	UCLA/Lick 3 m/spec.	1996 July 5	360
HD149307	1.139–1.315 (J)	UCLA/Lick 3 m/spec.	1996 July 5	10
Pistol Star	1.524–1.793 (H)	UCLA/Lick 3 m/spec.	1995 August 5	180
q3	1.524–1.793 (H)	UCLA/Lick 3 m/spec.	1995 August 5	240
Pistol Star	2.000–2.400 (K)	UCLA/Lick 3 m/spec.	1994 July 26	360
Pistol Star	2.000–2.400 (K)	UCLA/Lick 3 m/spec.	1995 August 5	180
Pistol Star	2.000–2.400 (K)	UCLA/Lick 3 m/spec.	1996 July 5	180
Pistol	2.000–2.400 (K)	UCLA/Lick 3 m/spec.	1996 August 20	360
q3	2.000–2.400 (K)	UCLA/Lick 3 m/spec.	1996 July 3	1200
HD163318	2.000–2.400 (K)	UCLA/Lick 3 m/spec.	1996 July 3	30
Pistol Star/Pistol	1.801–1.960	CGS4/UKIRT/$m = 2$[d]	1996 April 26	192
Pistol Star	2.106–2.263	CGS4/UKIRT/$m = 2$	1996 April 26	240
Pistol Star/Pistol	4.02–4.08	CGS4/UKIRT/$m = 13$	1997 July 13	288

[a] UCLA double-beam infrared camera (McLean et al. 1993, 1994).

[b] This filter has a central wavelength of 3.597 μm and $\Delta\lambda_{\rm FWHM} = 0.076$ μm, as measured in our own transmission plot.

[c] In speckle mode (Matthews et al. 1996).

[d] Grating order number. The "m = 2" observations were taken with the 150 l/mm grating while the "m = 13" observations were taken with the echelle. All CGS4 data were taken with the "short" camera.

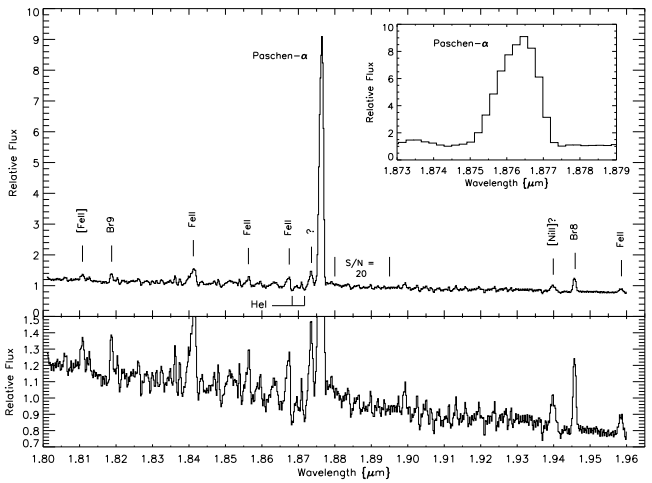

FIG. 2a

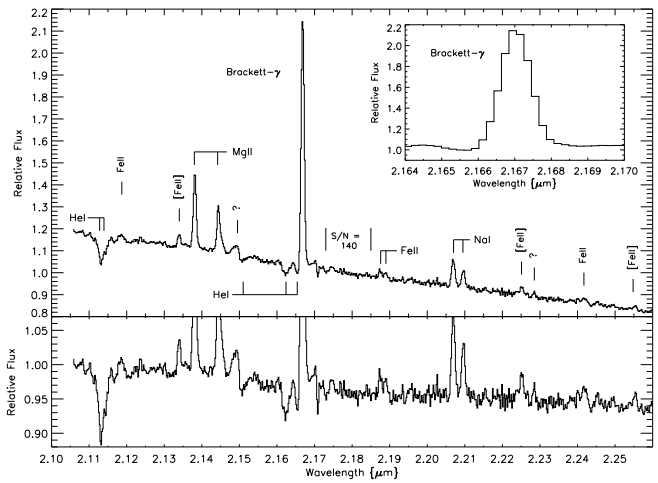

FIG. 2b

FIG. 2.—(*a*) Dereddened moderate-resolution spectrum ($R = 3000$) of the Pistol Star near the Paschen-α line. The bottom plot shows the spectrum at an expanded scale. Very sharp features, especially between 1.845 and 1.875 μm, are due to imperfect atmospheric correction. (*b*) Dereddened moderate-resolution spectrum ($R = 3000$) of the Pistol Star in the *K*-band. The bottom plot shows the spectrum divided by a straight line fit and at an expanded scale.

metry obtained on 1994 June 20 (FMM95). To compensate, we adjusted the *H*- and *K*-band zero points until the average photometry for the massive stars in the cluster matched the values in the older data. We fix the present error at ± 0.2 mag for all bands.

2.2. *Spectroscopy*

Low-resolution spectra were obtained with the UCLA double-beam near-infrared camera, which gives $R = \lambda/\Delta\lambda_{\rm FWHM,slit} \approx 525$ ($\Delta V_{\rm FWHM,slit} \approx 570$ km s^{-1}) on the University of California Observatories' 3 m Shane telescope.

The moderate- and high-resolution spectra were obtained with the Cryogenic Grating Spectrometer 4 (CGS4) on the United Kingdom Infrared Telescope (UKIRT). The 150 line mm^{-1} grating was used to produce the moderate-resolution spectra, while the echelle grating was used for the high-resolution spectrum. The "short" camera was used in both cases, producing a plate scale of $1\farcs23 \times 1\farcs23$ pixel^{-1} (width $\times$ height) for the moderate-resolution spectra and $1\farcs00 \times 1\farcs50$ pixel^{-1} for the high-resolution spectrum. In both cases, the slit width was ~ 1 pixel. The final spectra were constructed from sets of six exposures, each taken after translating the detector by $\frac{1}{3}$ pixel with respect to the fixed grating. The final reconstructed spectra are sampled every $\frac{1}{3}$ resolution element and have an effective resolving power of ≈ 3000 ($\Delta V_{\rm res.elt} \approx 100$ km s^{-1}) for the moderate-resolution spectra and $\approx 16{,}000$ ($\Delta V_{\rm res.elt} \approx 18$ km s^{-1}) for the high-resolution spectrum.

Conditions were photometric on all nights during which UKIRT data were obtained. It is unusual, even on Mauna

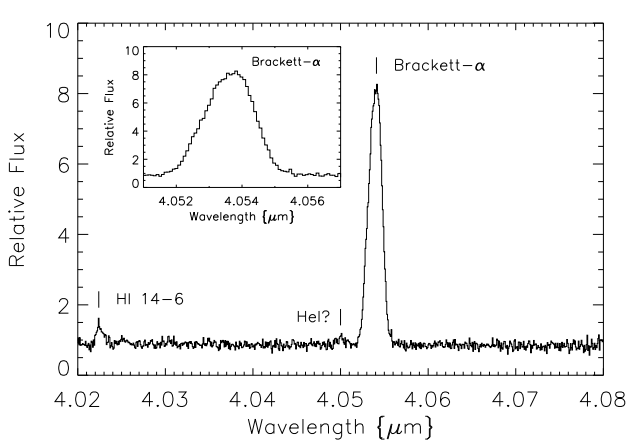

FIG. 3.—Normalized high-resolution spectrum ($R = 16{,}000$) of the Pistol Star near the Br-α emission line.

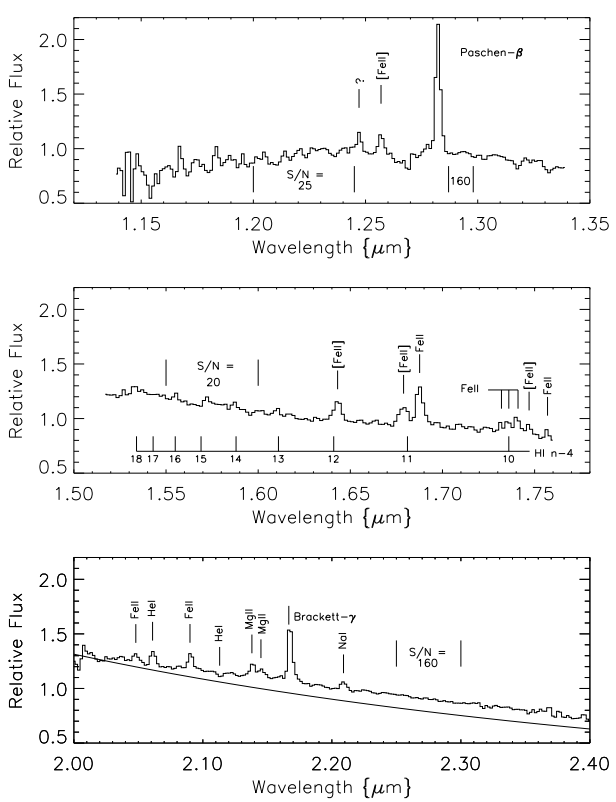

FIG. 4.—Dereddened low-resolution ($R \approx 525$) spectra of the Pistol Star in the *J*-, *H*-, and *K*-bands; $A_K = 3.2$ and $A_\lambda \propto \lambda^{-1.53}$ has been assumed. The absorption feature at 1.27 μm is due to imperfect atmospheric correction. The *K*-band spectrum was obtained on 1994 July 26. A blackbody curve ($T = 10{,}000$ K) is plotted in the bottom panel for comparison.

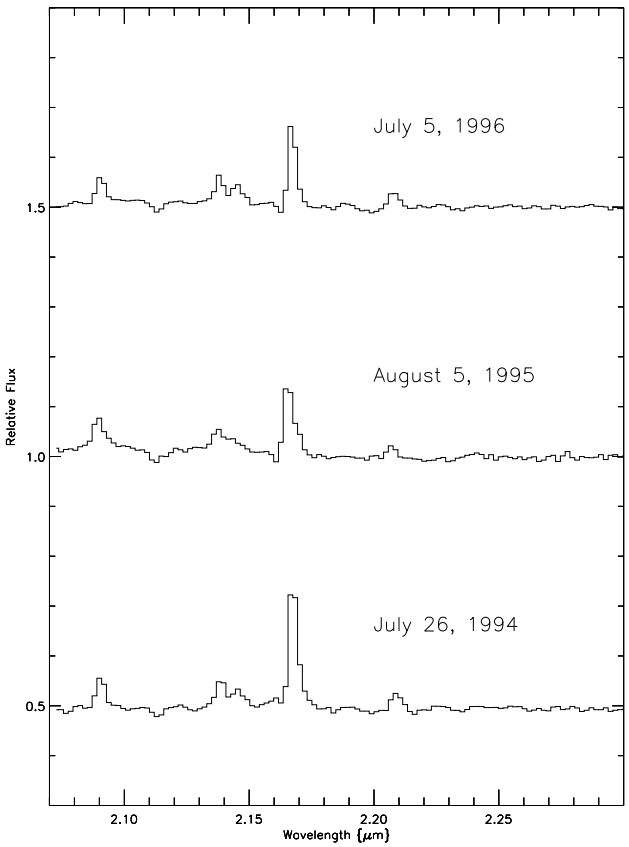

FIG. 5.—Normalized low-resolution *K*-band spectra of the Pistol Star. The equivalent widths for the Brackett-γ line are 21 Å (*bottom histogram*), 15 Å (*middle histogram*), and 14 Å (*top histogram*). The variations exceed the errors of 10% in the measurements.

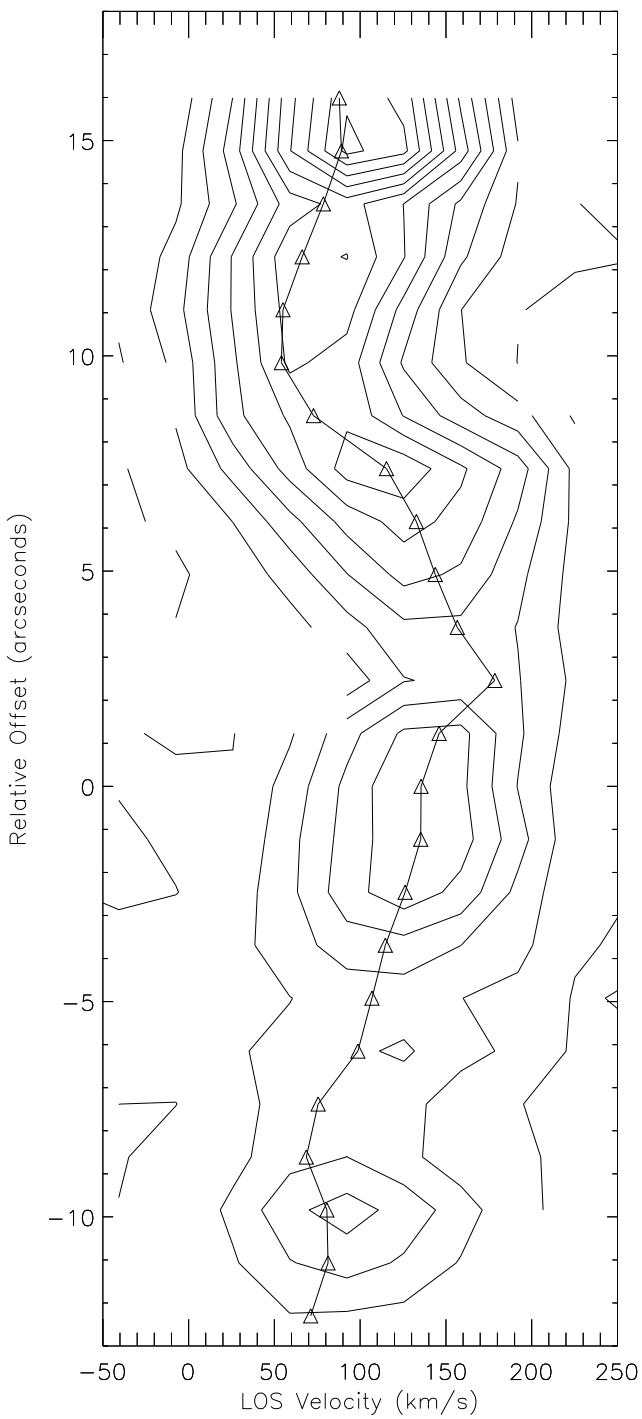

FIG. 6.—Declination-velocity plot of the Paschen-α line in Pistol. The triangles give the velocity centroid. The Pistol Star was located 7.″0 to the west of the center of the slit and is at zero offset north-south on the vertical axis. The background has been removed by subtracting an identical image with the object shifted in the north-south direction along the slit. The amount of the shift was less than the extent of the emission, so faint features may be uncertain.

Kea, that a good quality spectrum can be obtained in the 1.80–1.95 μm region. However, on the night of 1996 April 28, the water vapor column above Mauna Kea, although not extremely low, was stable during the measurements of the Pistol Star and the associated atmospheric standard. The strongest lines of water vapor, which absorbed about 95% of the continuum, are located just shortward of the Paschen-α line, in the 1.865–1.870 μm interval. We believe that the identified spectral features observed in this narrow spectral subinterval are real, as are those observed outside of it.

Between individual spectral images, each telescope was moved so as to position the star alternately at one of two locations along the slit. Subtraction of pairs of observations produced spectral images containing positive and negative spectra in two different rows on the array. The offsets were: $\sim$30″ north-south (low resolution), 12.″3 north-south (moderate resolution), and $\sim$16.″0 east-west (high resolution). In the case of the moderate-resolution spectra, only one of these spectra was used in the final coadded image.

In general, individual frames had "bad" pixels masked off, were flat fielded, and object − sky pairs were coadded to produce the final spectral images. The target spectra were then divided by the spectra of atmospheric standards to remove telluric features. A nearby Quintuplet star, "q3" (nomenclature from Moneti et al. 1994), was observed to provide an atmospheric standard for all the spectra, except in the *J*-band where an A2 star was used (HD 149307). The divided spectra were scaled by blackbodies having $T = 630$ K for q3 (see below) and $T = 8990$ K for HD 149307 (Theodossiou & Danezis 1991). The Paschen-β absorption line at 1.28 μm in the A2 star was first removed by linear interpolation. The highest quality *K*-band spectrum we have obtained for q3 is shown in Figure 1, confirming that

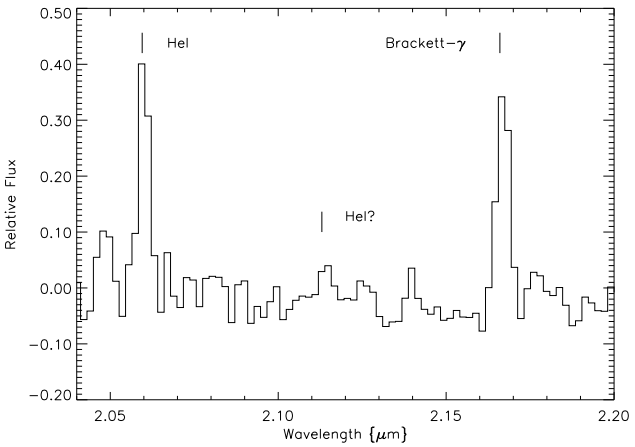

FIG. 7.—Dereddened *K*-band spectrum of gas in the Pistol. The Pistol Star was located 2.″6 to the west of the slit.

the intrinsic spectrum is essentially featureless. HD 163318 (A7 V; $T = 8200$ K) was observed as the atmospheric standard for q3.

The wavelength scales were determined by observing arc lamps for the low- and moderate-resolution spectra. The planetary nebula NGC 6572 was observed to provide a wavelength scale for the high-resolution spectrum; the data were corrected for the motion of the calibrator source, -8.7 km s^{-1} (Wilson 1953).

IRAF routines were used to extract and reduce the low- and moderate-resolution spectra, while Starlink's FIGARO package was used for these purposes for the high-resolution spectrum. The final reduced spectra of the Pistol Star are shown in Figures 2, 3, 4, and 5. Spectra of the Pistol Nebula are shown in Figures 6 and 7.

2.3. *Speckle Imaging*

We obtained *K*-band images using the facility near-infrared camera in speckle mode on the Keck I telescope (NIRC; Matthews & Soifer 1994; Matthews et al. 1996). The camera plate scale was 0.″020 per pixel, and the data were resampled to 0.″010 to aid in the data reduction. Five hundred specklegrams, each representing a 140 ms integration, were shifted and added to construct the final image. The point-spread function in the resultant image has $d_{\rm FWHM} \approx 0.''050$, the diffraction limit, and the first Airy ring can clearly be seen in Figure 8*a*. See Ghez et al. (1998) for more details on the data taking and reduction procedures. Figure 8*b* has been derived from the data in Figure 3*a*. It shows the minimum difference in *K*-band magnitude between primary and secondary components in the system as a function of distance between the two components.

3. STELLAR SPECTRUM

The spectra in Figures 2, 3, and 4 contain many emission lines of H I, Mg II, Na I, forbidden and permitted Fe II, absorption and emission lines of He I, and several unidentified lines. Table 2 gives a complete list of observed lines. The H I and He I lines come from the stellar wind/photosphere (see below). The Mg II lines are excited by Lyβ fluorescence in the wind, while the Na I lines are generated either far

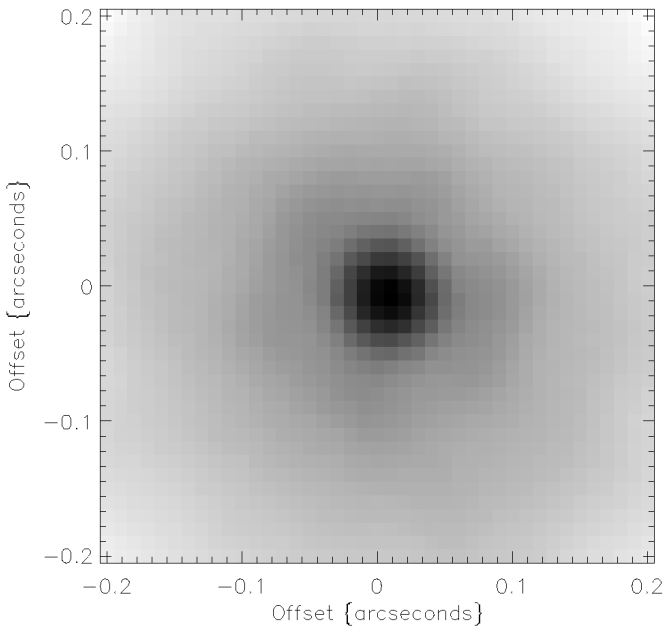

FIG. 8*a*

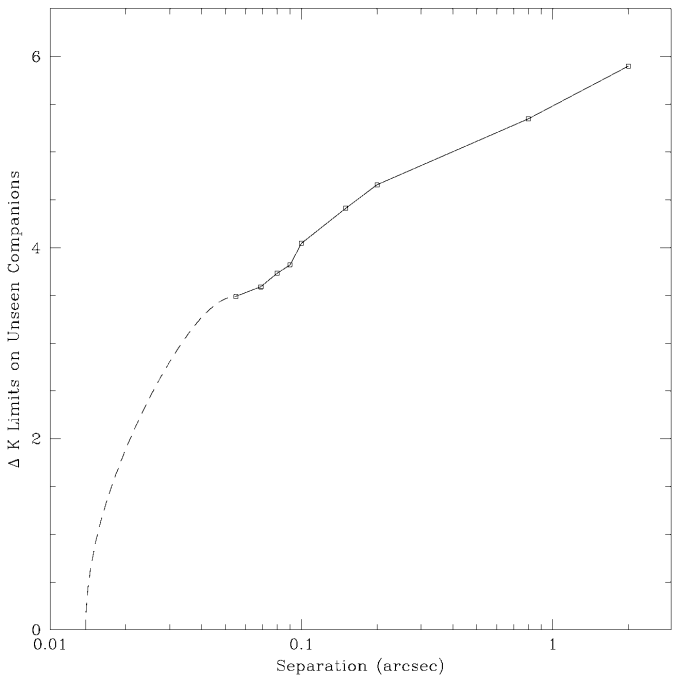

FIG. 8*b*

FIG. 8.—(*a*) Shifted and added *K*-band image. (*b*) Plot of ΔK vs. distance from the Pistol Star. This plot shows the minimum *K*-band magnitude difference between the Pistol Star and any companion as a function of distance from the Pistol Star. The analysis calculates the maximum intensity that a companion could have and still be consistent with the spatial power spectrum observed in the final reconstructed image shown in (*a*). The dotted curve extends the data to below the Rayleigh criterion diffraction limit. The limit for a primary and secondary of equal brightness is at 14 mas, or 110 AU.

TABLE 2

SPECTRAL LINES

Ion	Transition[a]	Vacuum Wavelength (Å)	Observed Centroid (Å)	V_{LOS} (km s^{-1})	W (Å)	ΔV_{FWHM} (km s^{-1})
?	...	...	12,471	...	4.9	...
[Fe II]	$a\,^6D_{9/2}$–$a\,^4D_{7/2}$	12,570.2	12,569	...	4.8	...
H I	3–5 (Paschen-β)	12,821.5	12,823	...	33.6	...
[Fe II]	$a\,^4F_{9/2}$–$a\,^4D_{7/2}$	16,440.0	16,431	...	9.3	...
[Fe II][b]	$a\,^4F_{7/2}$–$a\,^4D_{5/2}$	16,773.3	16,789	...	9.4	...
Fe II	$z\,^4F_{9/2}$–$c\,^4F_{9/2}$	16,877.8	16,876	...	17.8	...
Fe II[c]	$z\,^4D_{7/2}$–$c\,^4P_{5/2}$	17,343.2	...	...	...	...
Fe II[c]	$z\,^4D_{7/2}$–$c\,^4F_{7/2}$	17,418.8	...	...	...	...
[Fe II][c]	$a\,^4F_{3/2}$–$a\,^4D_{1/2}$	17,454.1	...	...	...	...
Fe II[c]	$z\,^4D_{7/2}$–$c\,^4F_{5/2}$	17,556.5	...	...	...	...
[Fe II][b]	$a\,^4F_{7/2}$–$a\,^4D_{7/2}$	18,098.8	18,108.9	167	2.0	188
H I	4–9 (Brackett–9)	18,179.0	18,188.7	159	2.0	127
Fe II	$z\,^4F_{7/2}$–$c\,^4F_{7/2}$	18,402.6	18,412.1	155	8.6	299
Fe II	$z\,^4F_{7/2}$–$c\,^4F_{5/2}$	18,556.4	18,563.9	122	3.3	184
Fe II	$z\,^4D_{5/2}$–$c\,^4F_{5/2}$	18,663.9	18,675.7	195	5.2	223
He I	$3\,^3D$–$4\,^3F$	18,690.4	18,683.4	...	−2.6	...
He I	$3\,^1D$–$4\,^1F$	18,702.2	18,718.4	...	−0.5	...
?	...	...	18,736.0	...	4.4	157
H I	3–4 (Paschen-α)	18,756.0	18,764.5	134	104	195
[Ni II]?	$a\,^4F_{9/2}$–$a\,^2F_{7/2}$	19,393.0	19,399.3	97	3.4	217
H I	4–8 (Brackett-8)	19,450.8	19,458.8	122	5.9	143
Fe II	$z\,^4F_{5/2}$–$c\,^4F_{7/2}$	19,577.4	19,585.9	130	2.5	245
[Fe II]	$a\,^4P_{5/2}$–$a\,^2P_{3/2}$	20,465.7	20,481	...	3.5	...
He I	$2\,^1S$–$2\,^1P^0$	20,586.9	20,612	...	5.8	...
Fe II[d]	$z\,^4F^0_{3/2}$–$c\,^4F_{3/2}$	20,893.8	20,904	...	6.5	...
He I	$4s\,^3S$–$3p\,^3P^0 + 4s\,^1S$–$3p\,^1P^0$	...	21,135.2	...	−2.0	299
Fe II	$z\,^4D^0_{5/2}$–$c\,^4P_{3/2}$	21,176.7	21,187.4	152	0.6	255
[Fe II][e]	$a\,^4P_{3/2}$–$a\,^2P_{3/2}$	21,333.5	21,341.5	112	0.4	129
Mg II	$5s\,^2S_{1/2}$–$5p\,^2P^0_{3/2}$	21,374.8	21,382.9	114	2.9	127
Mg II	$5s\,^2S_{1/2}$–$5p\,^2P^0_{1/2}$	21,438.0	21,446.6	120	2.4	177
?	...	...	21,491.3	...	1.5	417[f]
He I	$4p\,^3P$–$7s\,^3S$	21,500.0	...	...	...	...
He I	$4d\,^3D$–$7f\,^3F^0$	21,612.7	21,625.1	172	−0.85	234
He I	$4f\,^1F^0$–$7g\,^1G + 4f\,^3F^0$–$7g\,^3G$	21,647.4	21,655.4	111	−0.32	109
H I	4–7 (Brackett-γ)	21,661.0	21,670.1	124	11.4	131
Fe II	$4p\,^2G_{7/2}$–$4d\,^2F_{5/2}$	21,862.3	21,876.1	189	0.31	115
Fe II	$f\,^4G_{5/2}$–$4p\,^4G_{5/2}$	21,884.3	21,890.8	89	0.24	121
Na I	$4s\,^2S_{1/2}$–$4p\,^2P^0_{3/2}$	22,062.4	22,070.8	114	1.6	148
Na I	$4s\,^2S_{1/2}$–$4p\,^2P^0_{1/2}$	22,089.7	22,097.8	110	1.0	150
[Fe II]	$a\,^2G_{9/2}$–$a\,^2H_{11/2}$	22,243.7	22,252.7	121	0.60	216
?	...	...	22,286.4	...	0.16	...
Fe II	$z\,^4D^0_{3/2}$–$c\,^4P_{3/2}$	22,407.6	22,417.6	134	0.6	256
[Fe II]	$a\,^2G_{7/2}$–$a\,^2H_{9/2}$	22,540.7	22,555.0	190	0.28	137
H I	6–14 (Humphreys-θ)	40,208.5	40,221.6	98	4	...
He I	4–5	...	...	...	<1	...
H I	4–5 (Brackett-α)	40,522.4	40,536.9	107	150	118

NOTES.—Errors in the equivalent widths are dominated by systematic effects, i.e., choice of the nearby continuum flux level. In all cases, they are thought be less than 10%. Line centroids and V_{LOS} have been corrected for Earth motion. Earth motion on April 26 and July 13 was +22.5 km s^{-1} and −11.8 km s^{-1} respectively, along the line of sight toward the Galactic center (positive means toward the GC). A negative equivalent width indicates absorption. The spectra for $\lambda < 1.8$ μm and 2.00 μm $< \lambda <$ 2.10 μm were taken with lower resolution, so the line centroids and widths are uncertain; we refrain from calculating V_{LOS} for lines in these ranges. The Earth was receding from NGC 6572 by 7.5 km s^{-1} at the time of observation.

[a] The lower energy level is listed first. Vacuum wavelengths were taken from Johansson 1978 for iron, Reader & Corliss 1980 and Najarro 1995 for H I and He I, and Bashkin & Stoner 1975 for Na I and Mg II.

[b] Calculated using the corrected energy of 2430.097 cm^{-1} for $a\,^4F_{7/2}$, as noted in Allen et al. 1985.

[c] We did not attempt to deblend the lines between 17,360 Å and 17,550 Å.

[d] We favor this identification for the line in accordance with the identifications of Altamore, Maillard, & Viotti 1994 and Hamann et al. 1994 in the spectrum of η Car. Allen et al. 1985 suggest that [Fe II] $a\,^4G_{7/2}$–$b\,^2G_{7/2}$ (20,908.0 Å) may contribute to the 2.09 μm line in η Car, but this line is redward of the line we observe.

[e] Allen et al. 1985 give possible contributions to this line in η Car from [Fe II] $b\,^4F_{5/2}$–$a\,^2F_{5/2}$ (21362.7 Å) and [Fe II] $b\,^4F_{9/2}$–$a\,^2F_{7/2}$ (21377.9 Å), but these lines are redward of the line we observe.

[f] A blend.

from the star where the temperature would allow neutral sodium to exist or in gas that is shielded from the stellar radiation by dust (McGregor, Hyland, & Hillier 1988). The He I line near 2.113 μm is seen in absorption, as it is in FMM95. The weak absorption lines just shortward of the Brackett-γ emission line are He I 4–7 components.

Two very weak emission lines ($W < 0.4$ Å) can be seen in the moderate-resolution spectrum near 2.189 μm (Fig. 2*b*),

confirming the detection in Timmermann et al. (1996). We refrain from identifying either of these lines as He II (λ_{vac} = 2.18906 μm; Garcia & Mack 1965) because that line would appear at 2.18986 μm, significantly redward of the observed lines, if redshifted like the other lines in the spectrum. In addition, a much higher stellar temperature than the spectrum otherwise indicates would be required to produce such a line. We prefer to identify the lines as due to Fe II, wherein the upper state of the longer wavelength transition may be populated by fluorescing Lyϵ photons, assuming the appropriate Doppler broadening (60 km s^{-1}) as produced by the velocity field. At 2.187 μm in η Car, Allen, Jones, & Hyland (1985) observe an "unidentified" line, which we also suggest is due to these same Fe II transitions.

The line near 2.149 μm (Fig. 2*b*), also seen in Timmermann et al. (1996), appears to be a blend and remains unidentified. Near 1.75 μm, there are also several blended emission lines (Fig. 2*a*), which are likely due to Fe II, [Fe II], and Brackett-10, similar to the lines that have been detected in WRA 751 (LBV) and S Dor (LBV) at higher resolution (Morris et al. 1996).

3.1. *Comparison to Other Stars*

Overall, the spectrum of the Pistol Star is similar to those of LBV and B[e] stars. Such stars have *K*-band spectra marked by strong Brackett-γ emission, Mg II and Na I emission, and Fe II emission (see WRA 751:LBV, AG Car:LBV, and GG Car:B[e] in Fig. 7 of Morris et al. 1996). HD 72754 (B2 Ia:pe) is a close analogue to the Pistol Star in its *K*-band spectrum, although it lacks the He I absorption lines and its Brackett-γ emission line is stronger. WRA 751 is probably the next closest analogue, although it lacks the Na I doublet near 2.21 μm. The Pistol Star is unique in its unidentified emission line near 2.149 μm.

While the Pistol Star and WRA 751 have many lines in common, their equivalent widths differ; however, this may be at least partly related to the variability of these stars (see below and Tables 5 and 6 in Morris et al. 1996). For instance, Morris et al. (1996) show varying equivalent widths for WRA 751. The low-resolution spectrum of WRA 751 (Fig. 6 of Morris et al. 1996) has much stronger emission lines than the moderate-resolution spectrum obtained $\sim$1 yr later.

The iron line emission of the Pistol Star is similar to what is seen in S Dor, although the latter has much stronger higher order Brackett-series emission (Morris et al. 1996). The Pistol Star spectrum is also similar to that of η Car, although the spectrum for the latter has much stronger H I and He I emission lines and weaker Fe II lines (Allen et al. 1985; Hamann et al. 1994).

3.2. *Spectral Variability*

The low-resolution *K*-band spectra (Fig. 5) demonstrate that the Brackett-γ line is variable. The equivalent width in this line varied by the following factors, where the factors are normalized to the 1998 April 26 data and the date that the data were obtained is in parentheses: 1.8 (1994 July 26), 1.3 (1995 August 5), and 1.2 (1996 July 5). We estimate an error of 10% for these equivalent width measurements. In principle, a variation in equivalent width could be due to a variation in the continuum, but the equivalent widths of other lines are not nearly as variable as that of the Brackett-γ line. The He I lines, which are relatively constant, are formed close to the photosphere, while the Brackett-γ line is formed in the stellar wind. Hence, the Brackett-γ variability may indicate changes in the ionization structure of the wind. Also, note that the Fe II lines are relatively constant. A similar difference in behavior between the Fe II lines and the Brackett-γ line was also noted for η Car (Hamann et al. 1994).

4. STELLAR PARAMETERS

Stellar parameters, such as luminosity and temperature, offer insight into the evolutionary history of the star. In this section, the photometry and spectra are corrected for extinction, and stellar parameters are inferred through the use of the wind/atmosphere models.

4.1. *Systemic Velocity and a Location at the Galactic Center*

The line-of-sight velocities for the Pistol Star, the Pistol Nebula, and some of the Quintuplet cluster stars suggest a common location at the Galactic center. The Paschen-α, Brackett-γ, and Brackett-α lines in the Pistol Star are redshifted by $\approx$130 km s^{-1} (LSR), confirming earlier lower resolution measurements (Figer 1995; FMM96). The Paschen-α line in the Pistol Nebula is similarly redshifted, $V_{LOS,Pistol} \approx 130$ km s^{-1} (see below), as are the H I radio recombination lines (Yusef-Zadeh, Morris, & van Gorkom 1989; Figer 1995; Lang et al. 1997). Figer (1995) measured velocities for "q8" and "q10" (nomenclature from Moneti et al. 1994), two emission-line stars in the Quintuplet, finding an average line-of-sight velocity of 138 $\pm$ 30 km s^{-1}. Their data were not corrected for Earth motion, but such a correction would amount to less than 5 km s^{-1}. The ages and line-of-sight velocities of the Pistol Star and the other Quintuplet cluster stars (FMM96) support the conclusion that they all form a true physical cluster near the Galactic center. Our extinction estimates (see below) also support an association between the Pistol Star and the Quintuplet cluster and a common distance to them, consistent with a location near the Galactic center. We assume a distance of 8000 pc to the Galactic center (Reid 1993).

4.2. *Extinction*

Okuda et al. (1990) estimate $A_V = 20$–25 for the five reddest Quintuplet members from the polarization-A_V relation. Glass et al. (1990) estimate $A_V = 22$ from their measurements of the $H-K$ color excess, $E_{H-K} = (H-K) - (H-K)_0$, for Quintuplet cluster stars q7 and q8 (in their nomenclature); however, they were assuming that those two stars are red giants (see below). FMM95 estimate $A_V = 19^{+7}_{-6}$ for the WC9 star they identified, by assuming that star has the same intrinsic $H-K$ as the average of other Galactic WC9 stars, a questionable assumption given the large variation in near-infrared excess from circumstellar dust emission for late-type WC stars. Cotera et al. (1996) find $A_K = 2.8$ for the Pistol Nebula by comparing their measurement of the Brackett-γ flux to the 6 cm flux; this is equivalent to $A_V = A_K/0.112 = 25$ according to Rieke, Rieke, & Paul (1989). We find $A_K = 2.7$ ($A_V = 24$) for the Pistol Nebula using the same technique and our own measurement of the Brackett-γ flux.

We can also estimate A_K from the color excesses of OB I stars in the Quintuplet (Figer, McLean, & Morris 1998). We find an average $(H-K)$ of 1.75 for those stars ($\sigma = 0.28$;

TABLE 3

VALUES FOR EXTINCTION CONVERSION FACTOR

Reference	X[a]	$A_{K,\mathrm{Quin}}$[b]	Comments
Becklin et al. 1978	1.29	2.31	...
Landini et al. 1984.....	1.42	2.56	...
Rieke et al. 1989	1.78	3.20	No fit
Rieke et al. 1989	1.81	3.26	Power-law fit, $A_\lambda \propto \lambda^{-1.53}$
Cardelli et al. 1989.....	1.50	2.70	No fit
Cardelli et al. 1989.....	1.69	3.04	Power-law fit, $A_\lambda \propto \lambda^{-1.63}$
Glass et al. 1990	1.33	2.34	...

[a] Conversion factor between E_{H-K} and A_K, i.e., $A_K = X\,E_{H-K}$.
[b] Average extinction to the Quintuplet cluster stars as given by the specified extinction law and the measured colors, where appropriate.

FMM96), remarkably close to the value of 1.77 found for q7 and q8 by Glass et al. (1990). Our value gives $E_{H-K} = 1.80$, assuming $(H-K)_0 = -0.05$ (Koornneef 1983) for OB I stars. This can be related to A_K through a conversion factor, i.e., $A_K = XE_{H-K}$, where $X = 1/(A_H/A_K - 1)$. Table 3 gives values for X from several extinction laws.

The Cardelli, Clayton, & Mathis (1989) law gives approximately the same extinction as was found using the $I_{\mathrm{Brackett}-\gamma}/I_{6\ \mathrm{cm}}$ ratio; however, the Rieke et al. (1989; hereafter RRP) law, which was based on Galactic center studies, gives an extinction that provides a better fit to our model spectral energy distributions (SEDs; see below).

We favor the RRP law because it gives the best fit to the observed SEDs of the hot stars in the Quintuplet cluster, including the Pistol Star. This law gives $A_K = 3.2 \pm 0.5$ ($A_V = 29 \pm 5$), where the error is set by the standard deviation of $(H-K)$ for the OB I stars in the Quintuplet cluster. The variation in $(H-K)$ for these stars is intrinsic to the apparent colors of the stars, i.e., it is not due to inaccurate photometry or confusion. This can be seen in K-band spectra, which show that $A_K = 3.2$ would overestimate the reddening to some of the stars, given the slopes in their dereddened energy distributions, which are greater than that of an infinite-temperature blackbody (Figer et al. 1998). We take this to indicate that there is some differential extinction across the field and that an extinction value for each star will have to be individually computed.

We reinvestigated the Glass et al. (1990) extinction estimate. Their star 7 is known to be a red supergiant, while their star 8 is a hot star (WN9/Ofpe). Using their photometry, and $(H-K)_0 = -0.05$ for q8, we find $E_{H-K} = -1.76$ and $A_K = 2.34$ ($A_V = 29$) using their extinction law. Using the RRP law would give $A_K = 3.13$ ($A_V = 29$), nearly identical to our own estimates.

It is important to note that our luminosity estimate is an explicit function of A_K and, thus, will be in error to the extent that the extinction law is uncertain. The uncertainty of ± 0.5 mag in A_K corresponds to an uncertainty of ± 0.2 dex in total luminosity.

4.3. *Stellar Atmosphere Models*

4.3.1. *Spectral Energy Distribution (SED)*

Table 4 gives observed and dereddened broadband photometry from this work and from Nagata et al. (1993). The dereddened fluxes are plotted in Figure 9, assuming $A_K = 3.2$, and compared to scaled blackbodies having $T = 2500$ K and $T = 18{,}000$ K. The temperature of the hot blackbody was chosen such that a hotter blackbody of any temperature would not differ by more than 1% in relative shape over the 1–10 μm range. The temperature of the cool blackbody was chosen to simulate a cool companion. The fit to the higher temperature blackbody curve is good in the upper panel, except at J, where the observed flux is less than the blackbody flux, and at N, where the observed flux is greater than the blackbody flux. Notice that the flux in the J-band spectrum (Fig. 4) also decreases toward shorter wavelengths, confirming the behavior of the J-band photometry. The fit to the 2500 K blackbody is quite good in the J- and H-bands, but it overestimates the flux at longer

TABLE 4

BROADBAND PHOTOMETRY IN MAGNITUDES[a]

Photometry	J	H	K	L	M[b]	N[b]
Nagata et al. 1993.....	12.32	9.13	7.51	6.31[c]	5.68	5.04
Dereddened[d]	4.26	4.27	4.31	4.37	4.77	3.01
This work	12.08	9.33	7.39[e]	5.93[f]	...	...
Dereddened[d]	4.02	4.33	4.19	4.02	...	...

NOTE.—The Nagata et al. 1993 photometry has errors of ± 0.1 for $JHKL$, ± 0.2 for M, and ± 0.1 for N. The errors in our data are ± 0.2 for all bands and are set by the uncertainty in the atmospheric extinction correction.

[a] Zero point fluxes are adopted from IRTF Observer's Manual (Tokunaga 1986).
[b] Obtained at a different time than when the JHK data were obtained.
[c] Average of two values obtained at different times.
[d] Assumes $A_K = 3.2$ and the extinction law of Rieke et al. 1989.
[e] Converted from H and K' using the relation in Wainscoat & Cowie 1992.
[f] nbL.

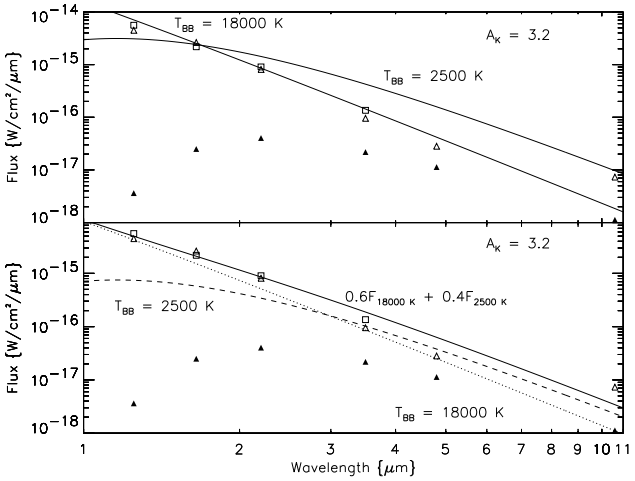

FIG. 9.—Near-infrared spectral energy distribution for the Pistol Star. The triangles and squares correspond to data from Nagata et al. (1993) and this work, respectively. Open symbols represent dereddened photometry. *Upper panel*: T = 18,000 K blackbody curve has been fit through the average dereddened photometry in the K-band, and a 2500 K curve has been fit through the average H-band photometry. *Lower panel*: dotted line represents a T = 18,000 K blackbody scaled to have 0.6 times the average dereddened flux in the K-band, and the dashed line represents a T = 2500 K blackbody scaled to have 0.4 times the average dereddened flux in the K-band. The solid line is a sum of the two blackbody curves. The temperature limit of the hotter blackbody was arbitrarily chosen such that a hotter blackbody would not differ by more than 1% in shape. The dereddening is discussed in the text.

wavelengths, especially at L and M. If the observed SED reflects an infrared excess from a cool companion or some nonstellar emission, then the flux from the wind/photosphere must not exceed the photometry in the J-band. If this were the case, then the luminosity of the star would be decreased by at least 2.5 times compared to the luminosity obtained for an intrinsic SED fit through the K-band photometry.

We attempted to vary the amount of extinction and the slope of the extinction law ($A_\lambda \propto \lambda^n$) to make a single-component blackbody fit the observed SED. A law that has $n \leq -1.8$ produces a dereddened K-band spectrum that is steeper than an infinite-temperature blackbody, assuming that $A_K = 2.7$. Values of A_K greater than 3.3 have a similar effect, assuming $n \sim -1.53$. A shallow law, i.e., $n > -1.5$, would decrease the dereddened J-band photometry for the Pistol Star, further increasing the difference between the blackbody model and the observations. If we assume that $A_{K,\text{Pistol Star}} = A_{K,\text{OB stars}} = 3.2$, then $n \approx -1.5$ to -1.6 provides the best overall fit to the SED (Figs. 10*a* and 10*b*).

We also tried to fit the SED with a two-component model consisting of a hot ($T > 18{,}000$ K) blackbody to represent the stellar photosphere and a cool (2500 K) blackbody to represent a cool companion or some nonstellar emission. In order to add these two components in the appropriate ratio, we attempted to estimate the maximum contribution that any cool blackbody could make to the observed SED. To do this, we estimated the deepest absorption in the He I 2.112 μm line produced by our wind/atmosphere models. Comparing this to the observed absorption shows that any non–wind/photosphere contribution to the SED, i.e., thermal emission from cool dust, cannot contribute more than 40% of the total flux to the apparent SED. Given this result, we plot the linear combination shown in the lower panel of Figure 9. This two-component model does not provide a fit that is much better than that provided by single-component models.

4.3.2. *Stellar Parameters*

To estimate the total luminosity of the star, we must first have an estimate of the temperature. The spectral lines provide sensitive diagnostics for this purpose. For the spectroscopic analysis, we proceed as described by Najarro (1995) and use the iterative, non-LTE method presented by Hillier (1987, 1990) to solve the radiative transfer equation for expanding atmospheres of early-type stars in spherical geometry, subject to the constraints of statistical and radiative equilibrium. Steady state is assumed, and the density structure is set by the mass-loss rate and the velocity field

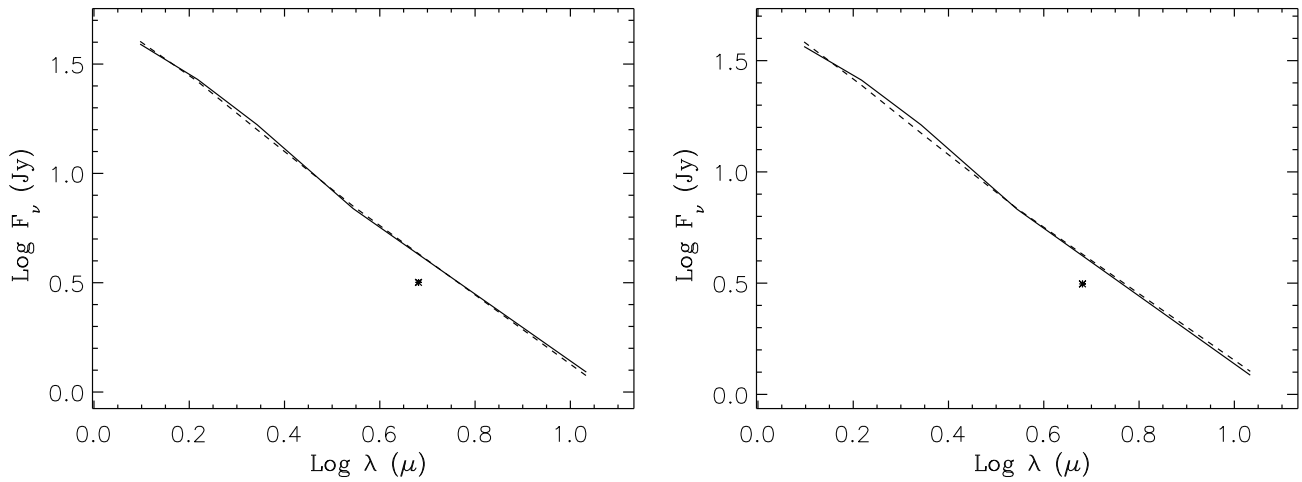

FIG. 10.—(*a*) Near-infrared spectral energy distribution (*dashed line*) fit by model L (*solid line*). The observed energy distribution is an average of the photometry in Table 4, dereddened assuming $A_K = 3.2$ (see text for extinction law). The M-band photometry, symbolized by a star, has been left out because it cannot be fit with any of our models. The extinction law in the 3–8 μm range was recently found to deviate from most extinction laws (see Lutz et al. 1996). (*b*) Model H, the rest is same as (*a*).

via the equation of continuity. The atmosphere is assumed to consist of hydrogen, helium, and nitrogen (N II–N III), where the latter is included to allow for its effect as a wind coolant (an abundance of $n_N/n_{He} = 10^{-2.30}$ was assumed). The model atoms consist of 15 H, 49 He I ($n \leq 10$) and 15 He II levels. The model is then prescribed by the stellar radius (R_*), the stellar luminosity (L_*), the mass-loss rate ($\dot{M}$), the helium abundance (n_{He}/n_H), and the velocity field [$v(r)$]. The modeled SED is scaled to the average dereddened K-band photometry given in Table 4.

We find two families of models that fit the SED and line profiles; their properties are listed in Table 5. The "L" model is representative of a family of models having relatively low temperatures, whereas the "H" model predicts higher temperatures. The model fits to the lines are shown in Figures 11*a*–11*g* for the L model. The H model produces similar fits, to within the errors of the models and the measurements, except for the Paschen-α line, for which the model flux is even less than that predicted by the L model.

The luminosity estimates in Table 5 are higher than the $10^{6.3}$ $L_\odot$ estimated in FMM95, primarily because of the difference in A_K. We can recalculate the luminosity using the revised A_K and the procedure in FMM95. They crudely estimated the bolometric correction BC_K ($M_{bol} = M_K + BC_K$) by taking the arithmetic mean of BC_K for LBVs in Blum, DePoy, & Sellgren (1995), finding $\overline{BC}_K = -1.4$. For $A_K = 3.2$, $M_K = -10.6$ (for $d = 8000$ pc), the luminosity is $10^{6.7}$ $L_\odot$. Averaging in data from LBVs in the Large Magellanic Cloud (McGregor et al. 1988) yields $\overline{BC}_K = -1.5 \pm 1.0$, where the error is the standard deviation of the sample. Using this new estimate, we find $L_{\text{Pistol Star}} = 10^{6.8(+0.3,\,-0.5)}$ $L_\odot$, remarkably close to the range of luminosities predicted by our wind/photosphere models. We can also estimate BC_K by assuming that the Pistol Star follows the same BC_K versus log T relationship that is followed by the LBVs in Blum et al. (1995). By taking their data for H-R Car, P Cyg, AG Car, and He 3−519, we find $BC_K = -7.1 \log T + 28.8$. Using an average temperature for the Pistol Star, log $T = 4.24$, we find $BC_{K_{\text{Pistol Star}}} = -1.6$, and $L_{\text{Pistol Star}} = 10^{6.8}$ $L_\odot$; this neglects minor differences in the definitions of T_{eff}. The fact that $\overline{BC}_K$ is nearly identical to BC_K inferred from the BC_K–log T relation is simply due to the Pistol Star having an "average" temperature for LBVs.

Cotera et al. (1996) estimated $L_{\text{Pistol Star}} = 10^{7.0}$ $L_\odot$ by fitting a blackbody curve through their near-infrared photometry. They estimated a temperature by finding that their H- and K-band spectra are similar to those of He 3−1191, which they assumed to be a B[e] star. As pointed out by FMM95, Le Bertre et al. (1989) have reclassified that star as a protoplanetary nebula, with $L < 10^3$ $L_\odot$. Despite this reclassification, the estimated temperature in Cotera et al. (1996), 20,000–30,000 K, is not much higher than the estimates from our models. Indeed, it is remarkable to note that the average of the earlier luminosity estimates ($10^{6.3}$ $L_\odot$ and $10^{7.0}$ $L_\odot$) is very near to the luminosity we now find from the L models.

Kudritzki et al. (1996) demonstrated an empirical and theoretical relationship between the "wind momentum rate," $\dot{M} v_\infty R^{1/2}$, and luminosity for stars whose winds are radiatively driven. The relation appears to hold for OBA and quiescent LBV stars in the Galaxy and the Magellanic clouds, although the scatter for the LBVs is rather large (Leitherer 1997). The wind momentum flux for the Pistol Star, as given by the parameters in Table 5, would indicate a luminosity of $\sim 10^{6.1}$ $L_\odot$ according to this relation (McCarthy et al. 1997). This type of estimate is actually an upper bound, considering that the models would give lower values of R and $\dot{M}$ for this luminosity. It is important to note that a relation of this form holds only for winds that are radiatively driven, and the scaling constants are applicable only within a particular subtype; i.e., main-sequence O stars have a different scaling constant than their more evolved descendants, i.e., Ofpe/WN9 stars. Also, the relation is likely to fail during outbursts when $\dot{M}$ increases by a few orders of magnitude over the quiescent rate, yet the stellar luminosity remains the same. In that case, the predicted luminosity would be much too high. The opposite is true in the case of the Pistol Star, for which the relation predicts a rather low luminosity compared to our other estimates; however, this relation has only recently been proposed, and its applicability to such high masses is uncertain. Through private communication with R. Kudritzki (1998), we learn that there is a change of curvature of the mass-to-light relationship toward very high masses. The effect would be to decrease the slope of the wind luminosity relation for high luminosity and high mass. Including this effect, we find good agreement with our inferred luminosity and mass-loss rate.

Figure 12 shows that the star lies above the observationally defined Humphreys-Davidson (HD) limit (Humphreys & Davidson 1979). A few other stars, e.g., η Car and HD 5980, are found in this region of the H-R diagram, and it is generally believed that such stars are unstable and susceptible to large eruptions in their outer atmospheres. This location in the H-R diagram is consistent with the Pistol Star being an LBV.

4.3.3. *Mid-Infrared Flux of the Pistol Nebula and Luminosity of the Pistol Star*

In principle, an important consistency check on the luminosity of the Pistol Star, L_*, is provided by the far-infrared luminosity of the surrounding nebula, L_{IR}. Using L_{IR} to

TABLE 5

MODEL PARAMETERS

Model	log ($L_*/L_\odot$)	log (T_{eff})	$R_{\tau=2/3}$ ($R_\odot$)	$\dot{M}$[a] (10^{-5} $M_\odot$ yr^{-1})	v_∞[b] (km s^{-1})	β[c]	N_{Lyc} (s^{-1})	n_{He}/n_H
L	6.61	4.15	340	3.8	95	1.75	$<3(10^{41})$	$0.13^{+0.03}_{-0.02}$
H.....	7.20	4.33	300	2.8	95	1.75	$4.4(10^{49})$	$0.12^{+0.03}_{-0.01}$

[a] Mass loss due to stellar wind.

[b] Terminal wind velocity.

[c] Wind velocity parameter. For large distances from the star, $v(r) \propto (1 - R_*/r)^\beta$. See eq. (2.7) of Najarro 1995 for a more general definition.

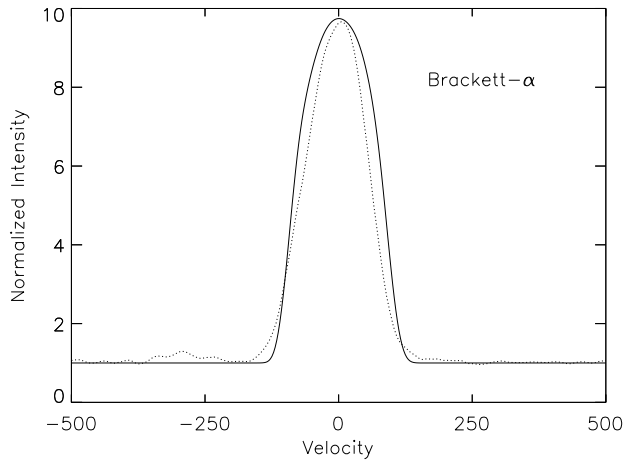

FIG. 11*a*

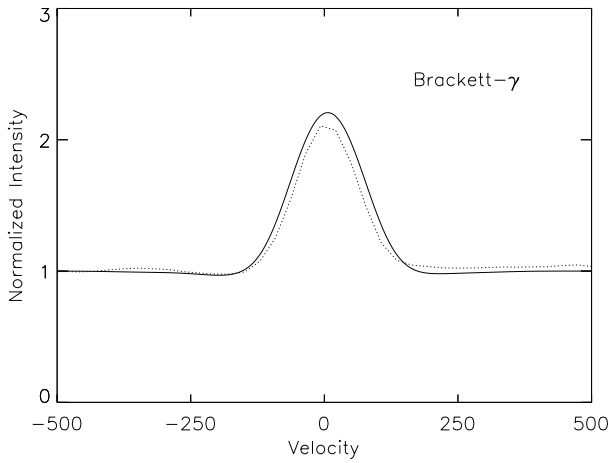

FIG. 11*b*

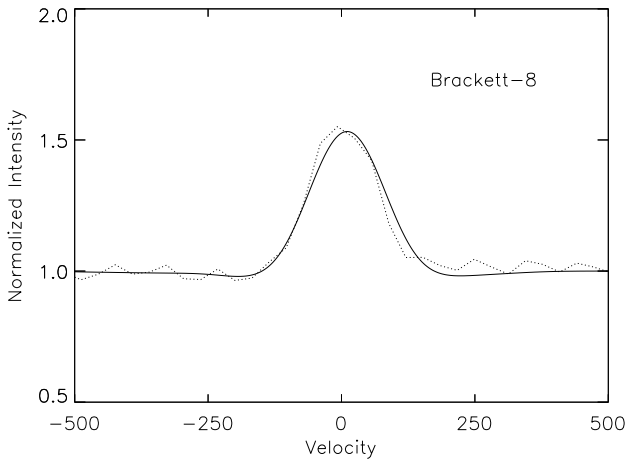

FIG. 11*c*

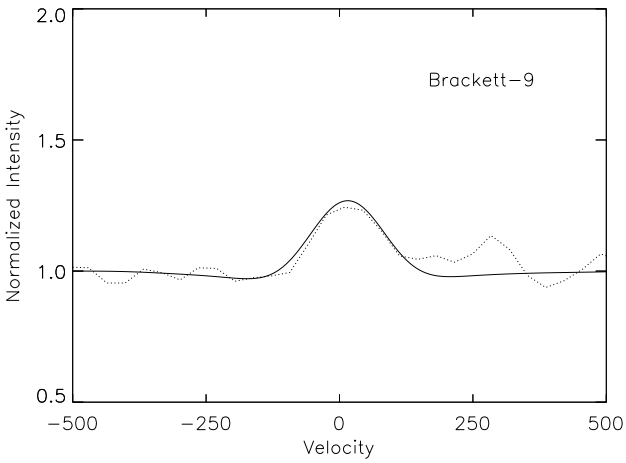

FIG. 11*d*

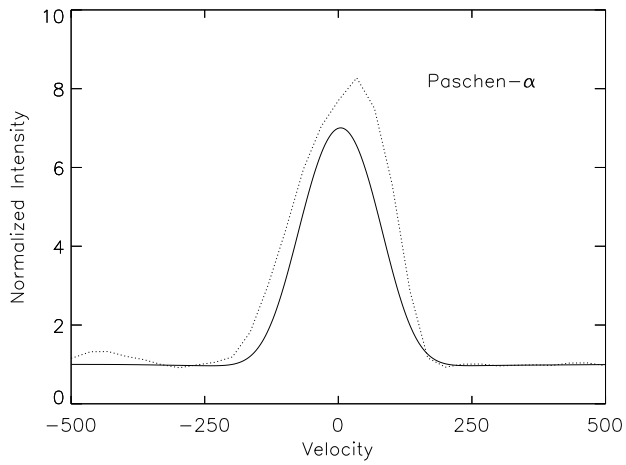

FIG. 11*e*

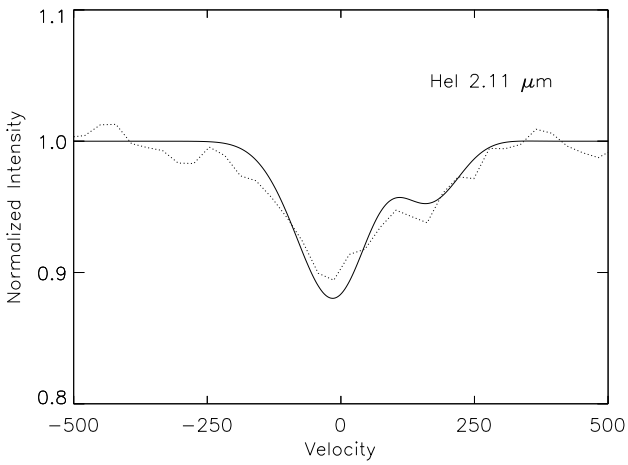

FIG. 11*f*

FIG. 11.—Model fit (*solid line*) to the data (*dotted line*) from the L model for (*a*) the Brackett-α line, (*b*) the Brackett-γ line, (*c*) the Brackett-8 line, (*d*) the Brackett-9 line, (*e*) the Paschen-α line, (*f*) the He I 2.11 μm line, and (*g*) the He I 2.16 μm line.

constrain L_*, however, requires estimation of three poorly known quantities: (1) the covering factor, f (the fraction of the total solid angle around the Pistol Star covered by a dusty portion of the nebula); (2) the mean radial absorption optical depth of the dust averaged over the stellar radiation field, $\tau_{\rm dust}$; and (3) the fraction of luminous energy absorbed by the dust in the Pistol Nebula, which originated in the Pistol Star. The entire Quintuplet cluster is presumably a nonnegligible contributor to the heating of the dust in the Pistol, depending on the line-of-sight displacement of the Pistol Star from the Quintuplet. Given all these uncertainties, the nebular luminosity serves primarily as a consis-

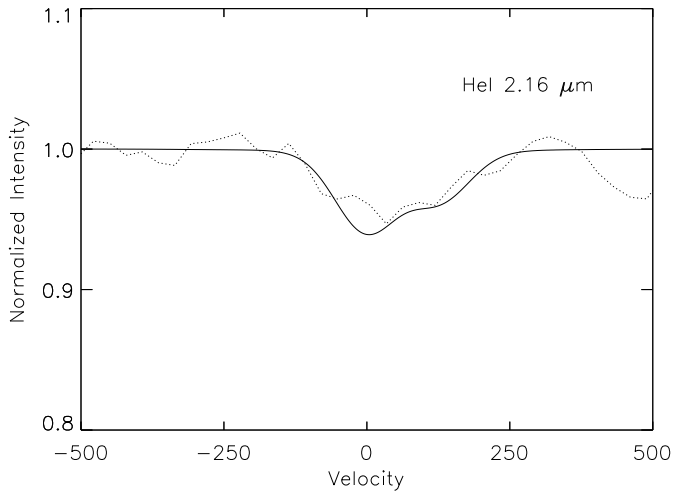

FIG. 11*g*

tency check on L_* rather than a particularly accurate estimate of it.

We approximate the Pistol Nebula as an incomplete spherical shell of covering factor f, outer radius r, and thickness Δr, so that the volume of the emitting region is then $(4\pi/3)[r^3 - (r - \Delta r)^3]f$. With r and Δr taken to be 0.6 and 0.3 pc, respectively, the radio flux of the pistol nebula (0.6 Jy at 6 cm; Yusef-Zadeh & Morris 1987) can be used to deduce the rms electron density, $n_{e,\mathrm{rms}} = 700 f^{-1/2}$ cm^{-3}, and the total nebular mass, $13.5 f^{1/2} M_\odot$.

An estimate of τ_{dust} requires knowledge of the gas-to-dust ratio, R, the typical grain dimension, a, and the absorption efficiency of the dust, Q. With $Q = 0.5$, $\tau_{\mathrm{dust}} = 0.09 f^{-1/2}(200/R)(10^{-5}\ \mathrm{cm}\ a^{-1})$.

In a 40″–45″ beam, Simpson et al. (1997) find that the luminosity of their source P6, centered on the Pistol Nebula, is $2.8 \times 10^5\ L_\odot$. This leads to an upper limit on L_* because some of the IR flux may have come from other

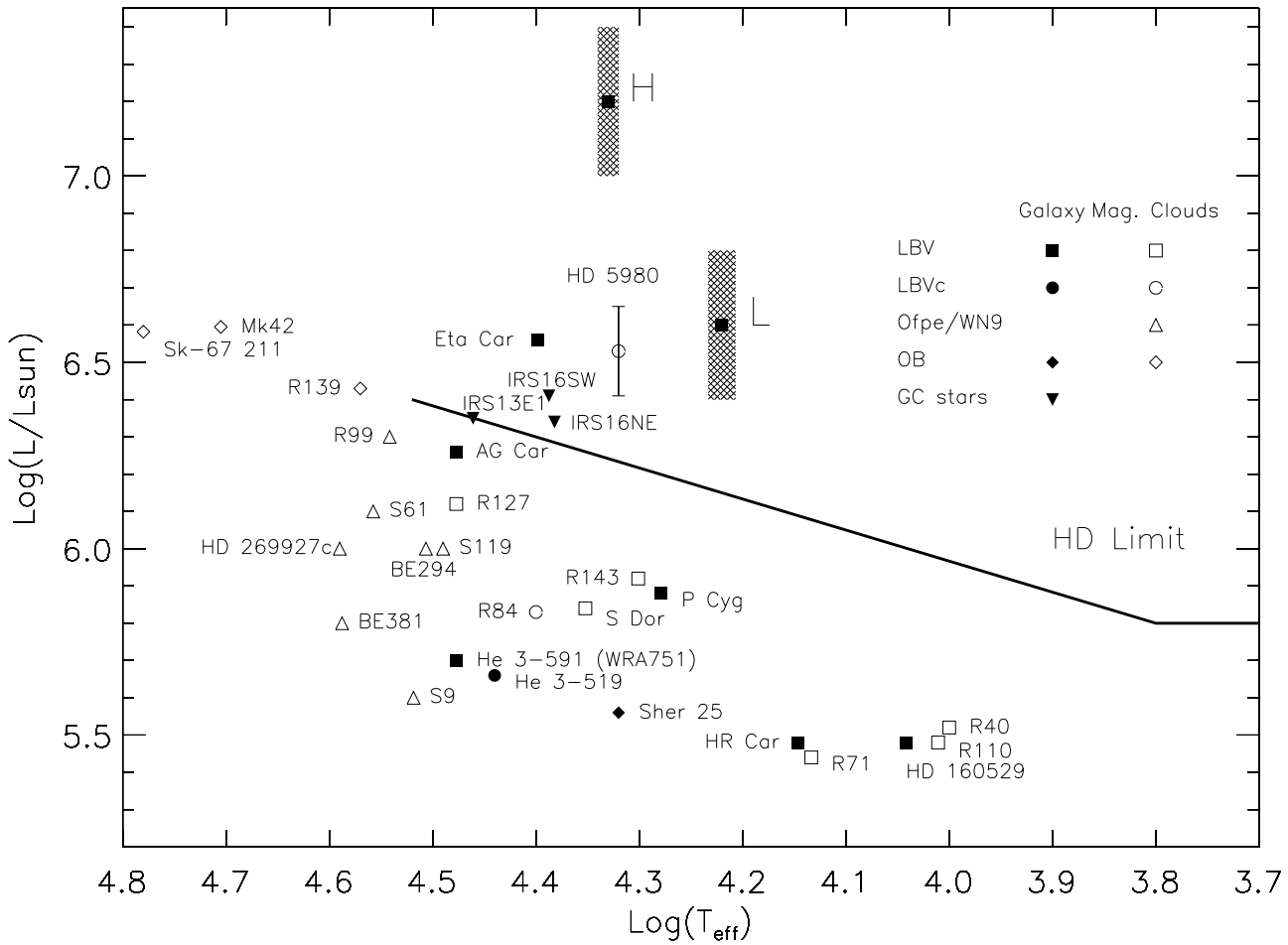

FIG. 12.—H-R diagram of the Pistol Star and other hot, luminous stars in the Galaxy and Magellanic Clouds, in quiescence. The data were taken from Humphreys & Davidson (1994), unless otherwise noted. When possible, the LBV data are at quiescence. LBVs are shown as squares, LBVc's as circles, Ofpe/WN9's as triangles, and OB stars as diamonds. Filled symbols are for stars in the Galaxy, and open symbols are for stars in the Magellanic clouds. LBVs make redward excursions in this diagram during eruption. For example, η Car might have been as cool as 5000 K during its last major eruption. See Humphreys & Davidson (1994) for more information concerning the locations of LBVs during eruption. Note that η Car may be a binary (Damineli et al. 1997). Data for Sher 25 in NGC 3603 were taken from Moffat (1983). Data for HD 5980 are from Koenigsberger, Auer, & Guinan (1997); it is not certain which component of this binary system is the LBV, so the luminosity spans a large range. Data for He 3 − 591 (WRA 751) are from Hu et al. (1990). Data for He 3 − 519 are from Smith et al. (1994). Data for R71 and R84 were taken from Crowther, Hillier, & Smith (1995). Data for Sk − 67°211 and Mk 42 were taken from Kudritzki et al. (1996). Data for the Ofpe/WN9 stars are from Pasquali (1997). Data for R139 (O7 Iafp) are from Walborn & Blades (1997). Data for the "GC stars" are from Najarro et al. (1997). Note that IRS 16NE has some LBV-like spectral characteristics (Tamblyn et al. 1996).

Quintuplet stars:

$$L_* < 2.8 \times 10^5\ L_\odot / f\tau_{\rm dust}$$
$$= 3 \times 10^6\ L_\odot\ f^{-1/2}(R/200)(a/10^{-5}\ \text{cm})\ .$$

We choose a filling factor of 0.4, noting that only one-half of the nebula appears to be ionized by the exciting source and that the gas appears to be clumped (see Fig. 13). We choose $R \sim 400$ as a conservative value for an LBV nebula (Nota et al. 1995) With these values, we find $L_* \lesssim 10^{6.7}\ L_\odot$. This is consistent with the luminosity we have deduced for the Pistol Star. Therefore, the luminosity of the nebula does not appear to be embarrassingly small.

4.4. *Multiplicity*

It is possible that the Pistol Star will be resolved into multiple components, as has been the fate of other luminous objects. Even η Car, long regarded as the most luminous single star known, has recently been claimed to be binary (Damineli, Conti, & Lopes 1997). Note that components in this binary are still very luminous, $\gtrsim 10^{6.3}\ L_\odot$. The brightest components of the R136 system, originally thought to be a single star (Weigelt 1981; Walker & O'Donoghue 1984), would have angular dimensions of 0.″6 (Panagia et al. 1991) at the distance of the Galactic center and thus would be resolved easily.

We have analyzed our reconstructed K-band image (Fig. 8*a*) and found that the Pistol Star does not have a companion that contributes one-half the light at a distance greater than 14 mas (110 AU) (Fig. 8*b*). A pair of equally massive stars at less than this separation would produce velocity shifts of greater than 75 sin i km s^{-1} and would have been detectable at inclinations of ≤ 20 degrees, except during small fractions of their orbital period. Pairs with mismatched masses could have higher relative velocities and, if the lower mass component were a line emitter, would be more easily detected. We conclude that it is unlikely that the Pistol Star is actually composed of two or more roughly

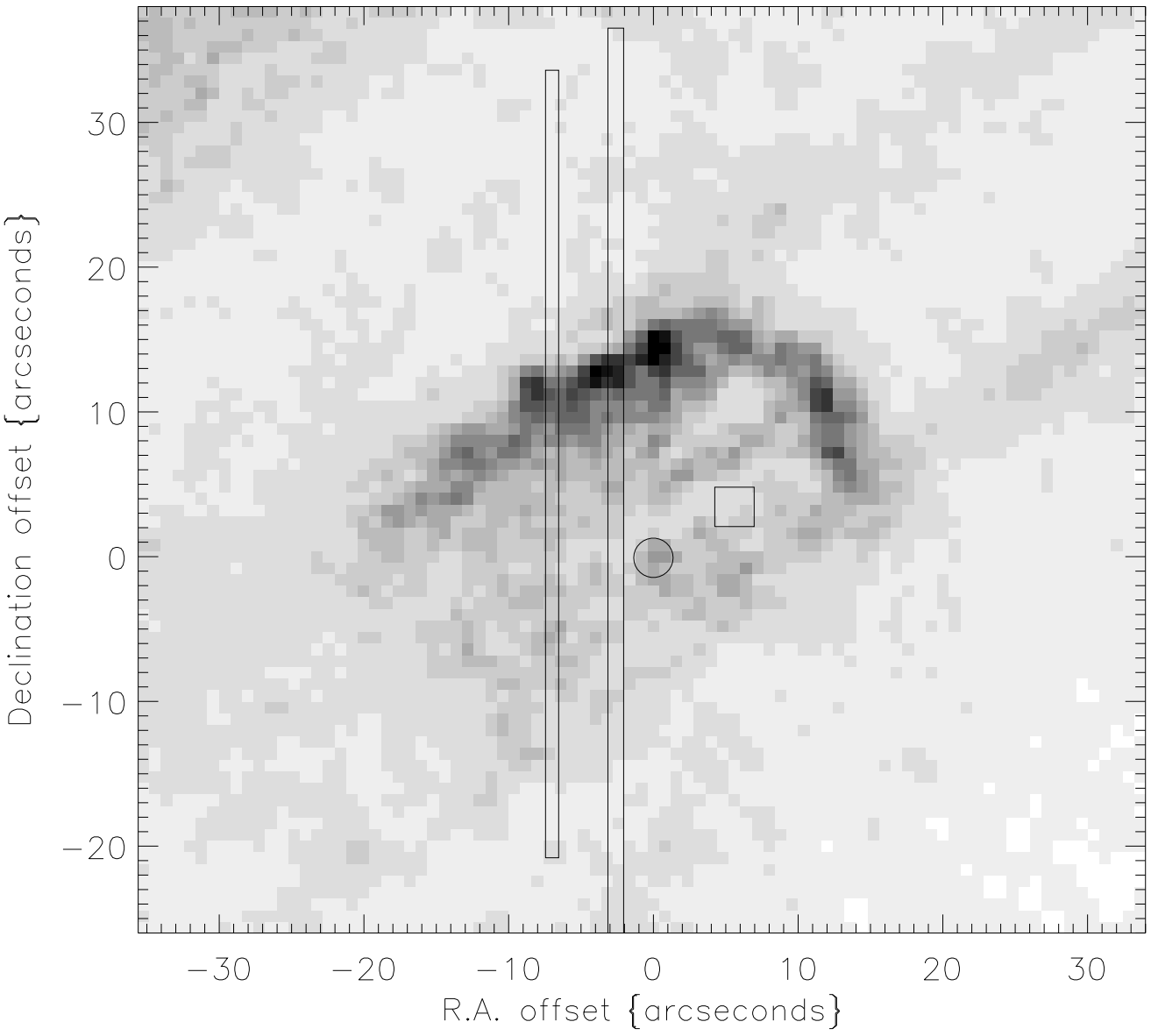

FIG. 13.—6 cm radiograph of the Pistol (M. Morris & F. Yusef-Zadeh 1997, private communication) taken with the VLA. The position of the Pistol Star is marked by a circle, and the position of qF 151 (WC8) is marked by a box. Notice that the radio emission peaks near the Pistol Star. The beam size is 1.″14 × 1.″05 (FWHM) with a position angle of 55.°9 east of north for the major axis. The rectangular boxes mark the slit locations referred to in the text.

equally luminous stars, but we cannot rule out that possibility.

4.5. *Spectral Classification and Variability*

Morris et al. (1996) have pointed out that the LBV classification (Conti 1984) should be reserved for stars that are truly luminous, blue, and variable, and that the Pistol Star does not yet appear to satisfy the latter condition. Our new spectroscopic data show that the star is spectroscopically variable (see Fig. 5); however, it has not been observed over a sufficient timescale and with the necessary photometric precision to ascertain whether it is as variable as known LBVs ($\Delta V \approx 2$ mag; Humphreys & Davidson 1994). The photometry in this paper shows that the star was 0.25 mag fainter in the *H*- and *K*-bands on 1996 July 4 than it was on 1994 June 20 (FMM95). Such a difference is consistent with the LBV classification, but it is barely outside the errors in the data. A more thorough observational program will be needed to determine whether the star is truly photometrically variable.

Morris et al. (1996) also argue that the *K*-band spectrum of the Pistol Star is consistent with it being classified as a B[e] star, as originally suggested by Cotera et al. (1996). The B[e] classification is reserved for B stars ($T_{\rm eff}$ = 10,000–30,000 K; Theodossiou & Danezis 1991) that have high luminosities, strong Balmer lines, Fe II and [Fe II] emission lines, double-peaked emission lines, and strong mid-IR excesses (Zickgraf et al. 1986). The Pistol Star satisfies the temperature, luminosity, and iron-line criteria; the Balmer series is inaccessible because of extinction. The star does not have significant mid-IR excess, separating it from most B[e] stars;

It is difficult to distinguish B[e] from LBV stars using *K*-band spectra alone. Morris et al. (1996) note that GG Car (B[e]) and AG Car (LBV) have quite similar *K*-band spectra. These similarities are probably not coincidental, and some B[e] stars may even be, or have recently been, LBV stars (see R4 in the SMC; Zickgraf et al. 1996). In fact, it is important to note that the term "LBV" is not a spectral classification, just as "Cepheid" is not a spectral classification. A star may be an LBV with a B0 I spectral classification just as a Cepheid may have an F5 III spectral classification at some point during its pulsation cycle.

Our suggestion that the Pistol Star be considered an LBV relies not only on its spectral appearance and spectral variability, but additionally on its position in the H-R diagram and its close proximity to the Pistol H II region (see below). One might suggest that even if the Pistol Nebula were created during an outburst from the star, the star might not currently be variable, and therefore it should not be considered an LBV now. This becomes a question of semantics, i.e., how recently should a star have been variable to be considered an LBV? We note that P Cygni, which exhibited great variability in its famous outburst of the 1600s, is now relatively quiescent (Israelian et al. 1996), although it was recognized as the "first" LBV (Humphreys & Davidson 1994).

5. STELLAR EVOLUTION MODELS

The mass-luminosity relation for evolved massive stars is not well determined observationally, but recently computed stellar evolution models have been successful in reproducing the massive star populations in the Galaxy and Magellanic Clouds. For the Pistol Star, we considered two sets of stellar evolution models: the "Geneva" models (Meynet et al. 1994), and our own new models that extend to very high initial masses. Both are computed for solar and twice solar metallicity, but the Geneva models further separate into "standard" and "2 ×" mass-loss models. The higher mass-loss models have been invoked, ad hoc, and assume mass-loss rates that are twice those observed (Garmany 1988); however, they can account for a high WNL/WR ratio and the presence of WC stars in starburst and WR Galaxies, as well as an extension (the "paunch") in the main sequence of massive stars ($M_{\rm initial} \sim 40\ M_\odot$) to cooler temperatures (Meynet 1995). Note that similar effects might be reproduced by including rotation (see below).

5.1. *Geneva Models*

Figures 14*a* and 14*b* show evolutionary tracks for massive stars according to the standard and $2 \times \dot{M}$ Geneva models. There are two tracks for each mass in each figure. The upper tracks (*dotted lines*) correspond to solar metallicity, and the lower tracks (*solid lines*) correspond to twice solar metallicity. The standard $\dot{M}$ models predict $M_{\rm initial} > 85\ M_\odot$ for $L \geq 10^{6.3}\ L_\odot$ for all metallicities yet modeled, $Z = 0.001$–0.04, and all evolutionary stages (Meynet et al. 1994). The $2 \times \dot{M}$ models predict $M_{\rm initial} \geq 120\ M_\odot$ for the same luminosity limit and $Z \geq 0.02$.

The models show that the effects of evolution dramatically alter the luminosity for massive stars. In high-metallicity environments, the luminosity tends to steadily decrease with age until the HD limit, while the opposite is true in low-metallicity environments; at this point, stars of all metallicities will drop dramatically in luminosity. For $M_{\rm initial} \geq 85\ M_\odot$ and $Z = 0.04$, the luminosity will tend to drop by at least an order of magnitude just 3 Myr after the star reaches the main sequence. In comparison, for $Z = 0.001$, a star with $M_{\rm initial} = 120\ M_\odot$ will increase in luminosity from $10^{6.2}\ L_\odot$ on the main sequence to a maximum of $10^{6.5}\ L_\odot$ 3 Myr later, assuming the $2 \times \dot{M}$ models. Shields & Ferland (1994) find $Z_{\rm GC} \sim 1$–$2\ Z_\odot$ according to their analysis of near- and mid-infrared emission lines in the central parsec, although Carr, Sellgren, & Balachandran (1996) recently found solar metallicity for red supergiants in the Galactic center. We assume $Z \geq 0.02$ in this paper.

If the Quintuplet is 3–5 Myr old (FMM96), and the Pistol Star is coeval with the cluster, then $M_{\rm initial}$ must have been even greater than $85\ M_\odot$ ($120\ M_\odot$) for the "standard" ($2\times$) $\dot{M}$ models; however, Figures 14*a* and 14*b* suggest that the Pistol Star is younger than 3 Myr. In fact, its age is less than one-half that value if we assume $Z = 0.04$, $M_{\rm initial} = 120\ M_\odot$, and the $2 \times \dot{M}$ Geneva models. The WC stars and the red supergiant in the Quintuplet have ages of >3.5 Myr and >4 Myr, respectively (Maeder & Meynet 1994), although the latter assumes solar metallicity.

5.2. *New Models—Slow Rotation*

Figure 15*a* shows our newly computed stellar evolutionary tracks with metallicities of 0.02 and 0.04 and initial masses in the range 60–300 $M_\odot$. These new models are calculated with a hydrodynamic stellar evolution code described in Langer et al. (1994), with an outer boundary condition adequate for spherically symmetric winds of arbitrary optical thickness (Heger & Langer 1996). Because of the lack of empirical mass-loss rates in the regime of our calculations, we applied the radiation-driven wind theory

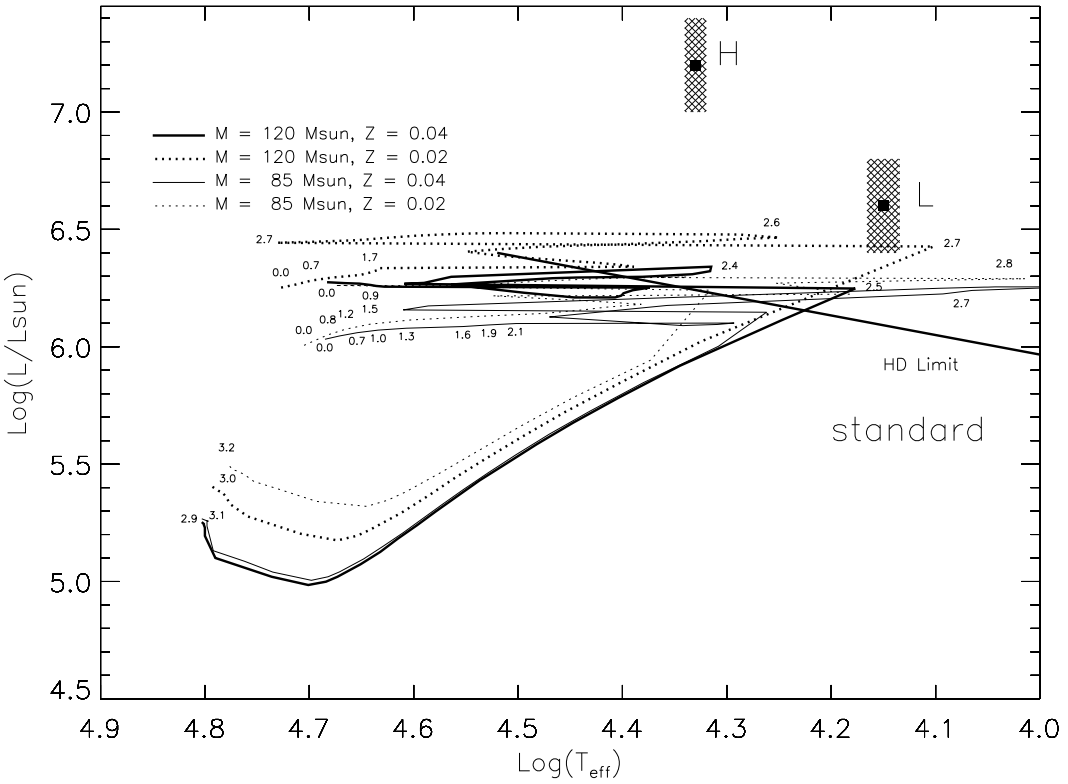

FIG. 14*a*

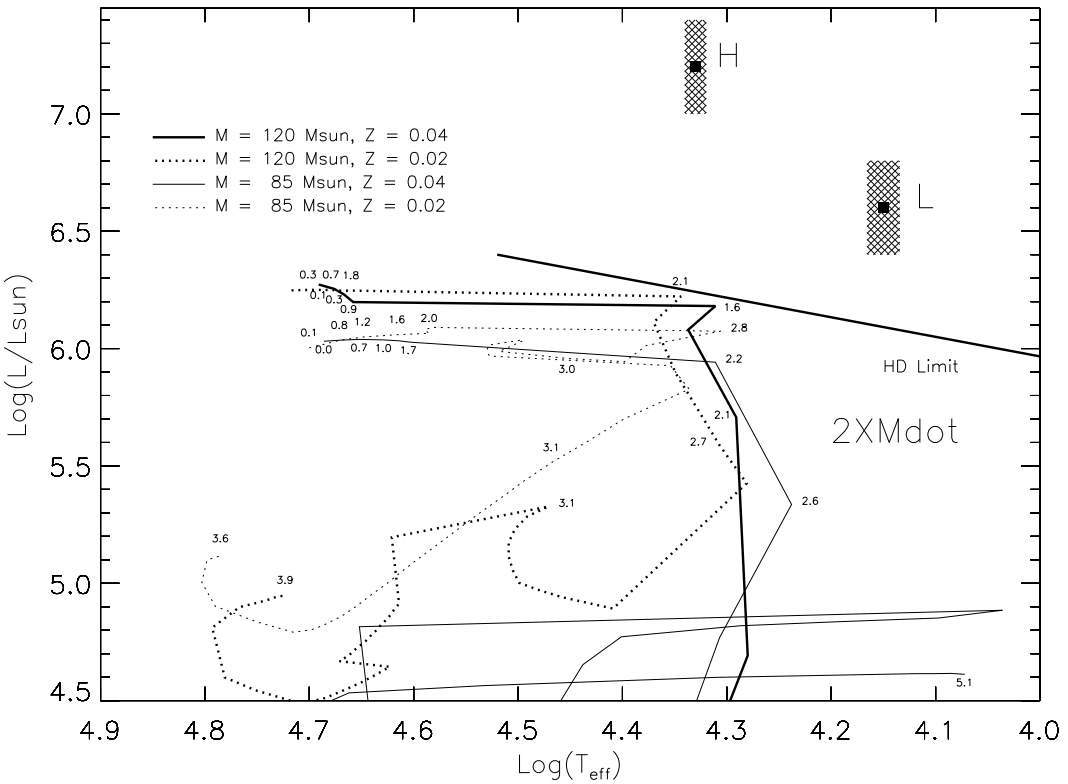

FIG. 14*b*

FIG. 14.—(*a*) Evolutionary tracks for stars with $M_{\rm initial} = 85\ M_\odot$ (*thin lines*) and 120 $M_\odot$ (*thick lines*) according to the "standard" $\dot{M}$ models in Meynet et al. (1994). There are two tracks for each mass, the upper track (*dotted line*) corresponding to solar metallicity and the lower track (*solid line*) corresponding to twice solar metallicity. Ages from the zero-age main sequence (ZAMS) in Myr are overplotted. The low- and high-luminosity model results for the Pistol Star are designated by the shaded regions. (*b*) Evolutionary tracks for stars with $M_{\rm initial} = 85\ M_\odot$ (*thin lines*) and 120 $M_\odot$ (*thick lines*) according to the $2 \times \dot{M}$ models in Meynet et al. (1994). There are two tracks for each mass, the upper track (*dotted lines*) corresponding to solar metallicity and the lower track (*solid lines*) corresponding to twice solar metallicity. Ages from the ZAMS in Myr are overplotted. The low- and high-luminosity model results for the Pistol Star are designated by the shaded regions.

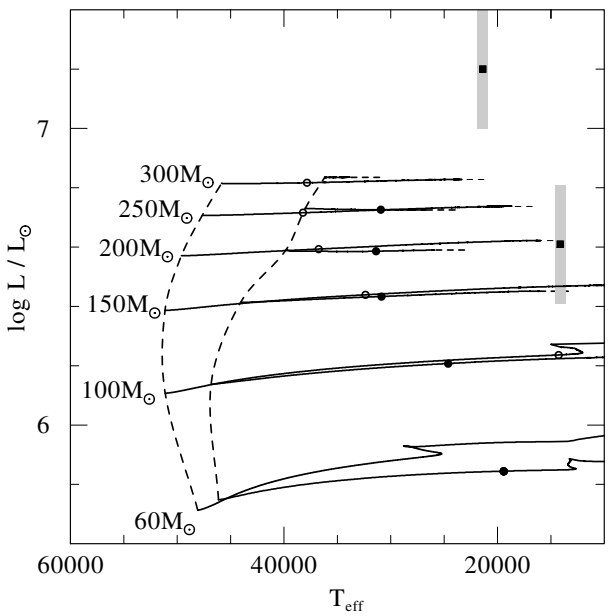

FIG. 15*a*

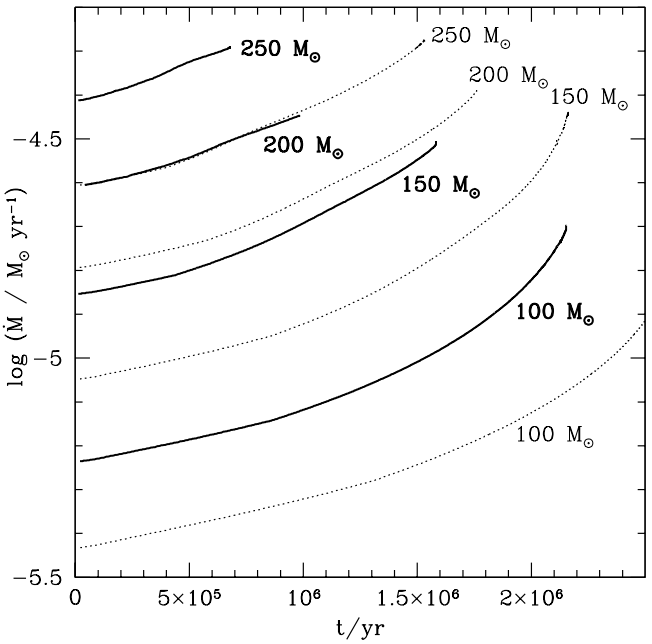

FIG. 15*b*

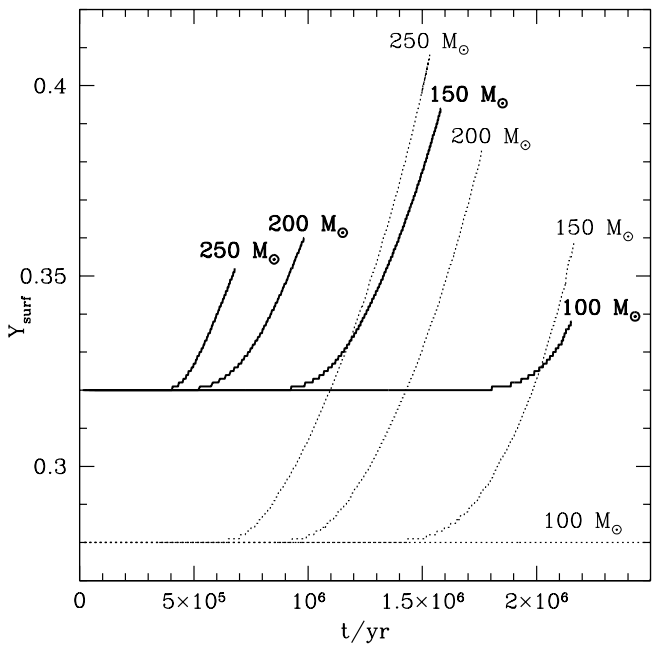

FIG. 15*c*

FIG. 15.—(*a*) Evolutionary tracks of our nonrotating models in the initial mass range 60–300 $M_\odot$ and metallicities of $Z = 0.04$ (*thick solid lines*) and $Z = 0.02$ (*thin solid lines*). Dashed lines mark the corresponding ZAMs. Filled and open dots on the tracks mark the first occurrence of nuclear processed material at the stellar surface, for $Z = 0.04$ and $Z = 0.02$, respectively. The low- and high-luminosity model results for the Pistol Star are designated by the shaded regions. (*b*) Mass-loss rate of our 100–250 $M_\odot$ stellar evolution models—calculated according to Kudritzki et al. (1989)—as function of time, for $Z = 0.04$ (*solid lines*) and $Z = 0.02$ (*dotted lines*). (*c*) Evolution of the surface helium mass fraction $Y_{\rm surf}$ as a function of time for the same stellar evolution models as shown in (*b*), for $Z = 0.04$ (*solid lines*) and $Z = 0.02$ (*dotted lines*).

according to Kudritzki et al. (1989) with wind parameters $k = 0.085$, $\alpha = 0.657$, $\delta = 0.095$, and $\beta = 1$ (Pauldrach et al. 1994); this parametrization accounts for the dependence of the mass-loss rate on luminosity, effective temperature, mass, and surface hydrogen mass fraction.

The mass-loss rate as a function of time for most of our models is shown in Figure 15*b*. Our models lose less mass than, e.g., those of Schaller et al. (1992); the 60, 100, and 150 $M_\odot$ sequences have, at core hydrogen exhaustion, 54, 84, and 110 $M_\odot$, respectively. The 200, 250, and 300 $M_\odot$ sequences are terminated at central hydrogen mass fractions of $X_c = 0.16$, 0.22, and 0.29, where the remaining masses are 158, 197, and 244 $M_\odot$, because of a hydrodynamic instability occurring at the stellar surface (see below). We note that a similar instability has recently been found in models of very massive stars of solar composition by Stothers & Chin (1997).

The reason for the smaller amounts of lost mass compared to Schaller et al. (1992) and Meynet et al. (1994) is understood as follows. Langer et al. (1994) and Meynet et al.

(1994) argued that the average amount of lost mass during core hydrogen burning for very massive stars (e.g., ~ 60 $M_\odot$) should be larger than the values resulting from semi-empirical mass-loss formulae (e.g., that of de Jager et al. 1988) or current radiation-driven wind models (see, e.g., Kudritzki et al. 1989) in order to obtain agreement with observed mean properties of very massive post–main-sequence objects, e.g., Wolf-Rayet stars. This apparent contradiction is resolved by considering the influence of rotation on the main-sequence mass loss of very massive stars. Langer (1998) finds that, depending on their initial rotation rate, 60 $M_\odot$ stars can end their core hydrogen burning with masses in the range 56–41 $M_\odot$, the largest value corresponding to the nonrotating case.

For the present investigation, i.e., trying to understand a very luminous but relatively cool star (the Pistol Star), we have to assume that its rotation rate is very small, since several investigations have shown that very massive rapid rotators do not evolve to cool surface temperatures because of rotationally induced internal mixing processes (Maeder 1987; Langer 1992; Fliegner & Langer 1995; Meynet 1998). Consequently, the use of $\dot{M}$ in the lower part of the possible range—e.g., that according to Kudritzki et al. (1989)—is appropriate here.

For the same reason, we did not invoke any "convective core overshooting." This has been applied in many massive star calculations in recent years in order to obtain a wider main-sequence band, the "paunch" (see Schaller et al. 1992). However, as rotationally induced mixing has a very similar effect (see, e.g., Langer 1992; Fliegner, Langer, & Venn 1996), we prefer the interpretation that the main-sequence widening is due to rotation and thus that the convective cores of nonrotating stars are not extended over the sizes predicted for them by the Schwarzschild criterion.

Furthermore, massive stars are supposedly becoming unstable when they approach or penetrate the Humphreys-Davidson limit in the H-R diagram. However, Langer (1997, 1998) has shown that, whichever instability mechanism causes the existence of the HD limit, its location in the H-R diagram must strongly depend on the rotation rate of the considered stars. For instance, if the Eddington limit is the physical cause of the HD limit, then the so called Ω limit, i.e., the corresponding instability limit for rotating stars (Langer 1997), is located at lower luminosities for more rapidly rotating stars. Or, vice versa, the instability limit for slowly or nonrotating stars is located at higher luminosity than that for stars rotating with the average rate.

Our finding that the most massive stellar models computed here become unstable at around $T_{\rm eff} \simeq 20{,}000$ K and $L \gtrapprox 10^{6.5}\ L_\odot$, together with the coincidence of the position of the Pistol Star with this point, leads us to propose the following scenario. The Pistol Star is unusually massive and may therefore have an unusual formation history. Apparently, it has obtained very little angular momentum, which perhaps allowed its mass to grow so much. Consequently, it evolved with less-than-average mass loss toward the cool side of the H-R diagram. During core hydrogen burning, it arrived at its Eddington limit and strongly increased its mass-loss rate. This is its present evolutionary stage. As it is still burning hydrogen in its core, the probability for the star to be found in this stage is not small. According to our models, its initial mass is 200–250 $M_\odot$, and its present age is in the range 1.7–2.1 Myr. The amount of mass lost prior to the occurrence of the surface instability is 42–53 $M_\odot$.

The surface helium mass fractions of our final models, shown in Figure 15*c*, are in the range $Y_{\rm surf} = 0.35$–0.40 (i.e., $n_{\rm He}/n_{\rm H} = 0.13$–$0.16$), with a corresponding nitrogen enhancement of a factor of ~ 10. Note that the mass-loss rate and surface helium abundance of our 200–250 $M_\odot$ models agree with the values obtained from the spectral analysis (see Table 5).

5.3. *The Pistol Star in the Context of Other Massive Stars*

The Pistol Star appears to have a very high luminosity, and, thus, a large present and initial mass. Table 6 shows that some stars in the Galaxy and Magellanic Clouds have similarly high luminosities, although none are as luminous as is the Pistol Star according to our H model. η Car and HD 5980 are closest to the Pistol Star in luminosity and temperature (also see Fig. 11); however, η Car might be

TABLE 6

STARS WITH $\log (L/L_\odot) > 6.30$

Star	MH98[a]	$\log (L_*/L_\odot)$	Reference
Pistol Star, H Model.....	...	7.20	This work
R136a1	3	6.69	Massey & Hunter 1998
Pistol Star, L Model	...	6.61	This work
Sk-67 211.....	...	6.58	Puls et al. 1996
η Car[b].....	...	6.57	Humphreys & Davidson 1994
R136a2	5	6.57	Massey & Hunter 1998
R134	4	6.57	Massey & Hunter 1998
R136a3	6	6.57	Massey & Hunter 1998
Mk 34	8	6.53	Massey & Hunter 1998
HD 5980[c].....	...	6.53	Koenigsberger et al. 1998
... .	10	6.45	Massey & Hunter 1998
Mk 42	2	6.45	Massey & Hunter 1998
Mk 39	7	6.41	Massey & Hunter 1998
... .	9	6.41	Massey & Hunter 1998
IRS 16SW	...	6.41	Najarro et al. 1997
IRS 13E1	...	6.35	Najarro et al. 1997
IRS 16NE	...	6.34	Najarro et al. 1997
Mk 37W.....	11	6.33	Massey & Hunter 1998

[a] Nomenclature from Massey & Hunter 1998.
[b] Damineli et al. 1997 suspect that η Car is binary.
[c] Hoffman et al. 1978 claim that HD 5980 is binary.

multiple (Damineli et al. 1997) and HD 5980 is an eclipsing binary (Hoffman, Stift, & Moffat 1978). If we interpret η Car as single, then our models would predict initial masses just as large as that predicted for the Pistol Star by our L model. Mk 42 and Sk -67 211 are just as luminous as the Pistol Star, assuming the L model. Their initial masses are likely to be $\gtrsim 150\ M_\odot$, although our models do not strictly include low-metallicity regions like those found in the Magellanic Clouds. Except for differences in metallicity, these two stars may be representative of the Pistol Star early in its life. AG Car and R127 are not quite as luminous as the Pistol Star (see Fig. 11), and both are hotter in quiescence; however, they make redward excursions in the H-R diagram, to temperatures $\lesssim 10{,}000$ K, bringing them much closer to the Pistol Star in the H-R diagram.

It is particularly interesting to note that several stars in the young cluster within the central parsec of the Galaxy (the "IRS" sources in Table 6) are nearly as luminous as the Pistol Star, assuming our L model. They are also relatively cool, placing them near, or above, the Humphreys-Davidson limit in the H-R diagram (see Fig. 11). Tamblyn et al. (1996) described a variety of evolved massive stars in the central parsec, suggesting that some are indeed LBVs (see § 4.4). The fact that both the Quintuplet cluster and the cluster in the central parsec contain very luminous evolved stars indicates that the two clusters have similar ages and evolutionary histories, a point that has been argued in FMM96.

In summary, there are several stars of luminosity comparable to that of as the Pistol Star if we assume our L model, but none are as luminous if we assume the H model. The young cluster in the central parsec of the Galaxy, in particular, contains a number of stars that can be considered to be in the Pistol Star's "peer group."

6. THE PISTOL NEBULA AS PHOTOIONIZED EJECTA

Many LBVs are surrounded by circumstellar ejecta, material that is removed from the stars during eruptive episodes of mass loss. These great eruptions may repeat every few thousand years over a period of several tens of thousands of years (Humphreys & Davidson 1994). Assuming a time-averaged mass loss of $2 \times 10^{-4}\ M_\odot\ \mathrm{yr}^{-1}$ over this period, the total mass lost in the LBV stage is $\approx 5\ M_\odot$, consistent with the fact that LBV nebulae (LBVN) generally contain a few solar masses of ionized gas (Nota et al. 1995).

6.1. *Morphology*

The Pistol Nebula surrounding the Pistol Star may be photoionized circumstellar ejecta (see Fig. 13). The line-of-sight velocity of the Pistol Star, ≈ 130 km s^{-1}, matches the average velocity of gas in the nebula (Fig. 6), and the Pistol Star is located roughly near the center of curvature of the bright ridges of emission in the surrounding gas. In addition, the star is coincident with a peak in the 6 cm flux (see Fig. 13). The general shape of the nebula does not necessarily require an ejection process, but it is remarkably similar in appearance to the ejecta around WR 136, the nebula NGC 6888 (Marston 1995). Several LBVN have elliptical shapes like the Pistol Nebula, and Nota et al. (1995) have summarized processes that might produce this morphology. One of these processes, wind-wind interactions, may be particularly relevant, given the many nearby stars with powerful winds.

6.2. *Mass*

Lang et al. (1997) estimate $M_{\mathrm{ionized}} \approx 11\ M_\odot$ in the Pistol Nebula. We recalculated this value according to

$$n_e = \frac{60(F_\nu)^{1/2}}{\phi^{3/2} d^{1/2}}\,, \tag{1}$$

where ϕ is the diameter of the nebula in degrees, F_ν is in Jy at 6 cm, and d is the distance to the nebula in pc (Kaplan & Pikelner 1970). Assuming $\phi = 0.^\circ0083$ ($r_{\mathrm{Pistol}} = 8000$ pc), and $F_\nu = 0.6$ Jy, we find $n_{e,\mathrm{rms}} = 700$ cm^{-3} and $M_{\mathrm{ionized}} \approx 15\ M_\odot$.

This analysis assumes that the gas is homogeneously distributed in a sphere, a questionable assumption given the knotty appearance of the emission (see Fig. 13). Consider an alternative geometry of a spherical shell with inner radius 0.5 pc and outer radius 0.6 pc. The emitting volume can be replaced by a homogeneous sphere having a radius of 0.45 pc, and equation (1) can be used to find $n_{e,\mathrm{rms}} = 1052$ cm^{-3} and $M_{\mathrm{ionized}} \approx 10\ M_\odot$.

In either case, the mass is relatively high in the context of LBVN, but more massive stars may lose more mass in the LBV stage (Humphreys & Davidson 1994), and the Pistol Star appears to be very massive. Could this much mass have come from the star's steady wind? Table 5 gives $\dot{M} \approx 4 \times 10^{-5}\ M_\odot\ \mathrm{yr}^{-1}$, a value that is in the range of mass-loss rates for quiescent LBVs (Nota et al. 1995). We can multiply this value by the dynamical timescale for the nebula. Assuming $r_{\mathrm{Pistol}} \approx 0.6$ pc and $v_\infty = 100$ km s^{-1} (Table 5), we estimate a dynamical time of ≈ 6000 yr and $0.2\ M_\odot$ lost in a steady wind. This is 50 times less than the amount necessary to account for the mass in the Pistol Nebula. This suggests three possibilities: (1) the star must have had a much higher $\dot{M}$ in the past, i.e., during one or more eruptions; (2) other nearby stars are contributing to the nebula through mass loss; and (3) the gas in the Pistol was swept up from the ambient interstellar medium.

One might expect that the ambient medium has a low density because it has been evacuated by the winds from O stars in the Quintuplet and then partially refilled by matter from stars with slower winds, i.e., the Ofpe/WN9 and WC9 stars. Even if the other stars collectively contributed 10 times the mass that could come from the Pistol Star, they would still contribute only $2\ M_\odot$ of mass that could be swept up, and that assumes that the mass could be focused into the morphology that is seen in the Pistol Nebula. These arguments favor possibility 1.

6.3. *Ionizing Flux*

FMM95 estimate that the Pistol Star produces 3.4×10^{48} Lyman continuum photons second^{-1}, roughly the number required to account for the radio flux from the Pistol Nebula. Our new estimates give a very large uncertainty for the Lyman continuum flux, from $<10^{40}$ to 2×10^{50} s^{-1}. Ionizing flux scales strongly with temperature for this region of parameter space; in fact, an increase of 2000 K in temperature for the low-temperature model would increase the ionizing flux to the value estimated in FMM95. Lang et al. (1997) estimate $N_{\mathrm{Lyc,Pistol}} = 5.6 \times 10^{48}$ s^{-1}, while Yusef-Zadeh, Morris, & van Gorkom (1989) estimate 3.9×10^{48} s^{-1}, both on the basis of the Pistol's radio flux. Considering the low-temperature model, the difference between the ionizing flux required to ionize the Pistol and

our estimate of what the star produces might be made up by the flux from nearby hot stars, i.e., qF 151 (WC8) (FMM96).

This difference might also be explained if the Pistol Star emitted a greater ionizing flux during the recent past. Meaburn et al. (1996) speculate that the ionized gas in the nebula surrounding P Cygni is currently recombining following a period of ionization. This lagging recombination is invoked quite often to explain the ionized gas around cool LBVs (Nota et al. 1995). The recombination timescale for hydrogen is $\lesssim 1.2 \times 10^5/n_e$ yr. If a similar scenario is true for the Pistol Star/Pistol system, then the gas would have last been ionized ~ 170 yr ago assuming $n_e = 700$. If such an episode of increased ionization occurred, it probably would not have coincided with the ejection of the bulk of the gas, because the expansion velocity would have to have been an unlikely ≈ 3000 km s^{-1} for the gas to now be located at its observed separation from the star.

6.4. *Velocities*

The velocities in the gas (see Fig. 6) vary smoothly along the north-south direction. The maximum of 179 km s^{-1} is near the declination of the Pistol Star, while the minima of 55–70 km s^{-1} are at $\approx \pm 10''$ relative to the star. The average velocity is 103 km s^{-1} along the slit. The general velocity profile is similar to that seen in the H92α line (see Fig. 10*a* of Lang et al. 1997); however, the velocity extremes in our data are greater. Although the velocities are symmetric in the north-south direction, the data are not well fit by a simple spherically expanding shell of gas. For such a simple geometry, one would expect to see a double-peaked emission line, equally spaced in velocity about the systemic velocity of the system. The two lines would have the greatest separation at the location of the star and would have the systemic velocity toward the nebular limbs. This type of pattern is well illustrated by the nebula surrounding the LBVc He 3−519 (Smith, Crowther, & Prinja 1994). Similar expanding shell geometries are found around the majority of LBVs (Nota 1995). Lang et al. (1997) do fit a double H92α line in the eastern side of the Pistol, but the line is single elsewhere in the nebula. The velocity field of the Pistol Nebula clearly warrants further study.

6.5. *Composition and Excitation*

Figure 7 shows that the 2.058 μm He I line and the Brackett-γ line have equal strength. The flux ratio of these lines can be used to estimate the helium abundance in the Pistol Nebula. DePoy & Shields (1994) calculated expected values of $F_{2.058\ \mu m}/F_{2.166\ \mu m}$ for a range of nebular densities and stellar temperatures of the exciting star, assuming solar abundance in the gas. The 2 ^1P level of He I can be populated by (1) recombinations to neutral helium, (2) pumping of the 2 ^1P level by resonant scattering of 584 Å photons (1 ^1S–2 ^1P), and (3) collisional depopulation of the 2 ^3S level.

The number of ionizations, and thus recombinations, to neutral helium increases with increasing temperature of the exciting star; however, at a high enough temperature, helium is mostly doubly ionized and recombinations will be to singly ionized helium. Most of the recombining electrons will decay to the 2 ^1P level where they have a 99.9% chance of further decaying to the 1 ^1S level as opposed to the 2 ^1S level. A 584 Å photon is emitted for each 1 ^1S–2 ^1P transition, but this photon will probably be immediately absorbed by a nearby neutral helium atom, assuming that the gas is optically thick to this radiation and that the photon is not absorbed by dust or H I. $F_{2.058\ \mu m}/F_{2.166\ \mu m}$ increases with nebular density and peaks at a temperature of $T_{\rm eff} \approx 40{,}000$ K for the exciting star.

Transforming equations (4) and (5) from Doherty et al. (1994), we find

$$\frac{N^{\rm He}_{\rm Lyc}}{N^{\rm H}_{\rm Lyc}} = \frac{I_{\rm He\ I\ 2.058\ \mu m}}{I_{\rm Br\gamma}} \frac{\alpha_B({\rm He}^+)}{\alpha_B(H^+)} \frac{\alpha_{\rm Br\gamma}}{\alpha_{\rm He\ I\ 2.058\ \mu m}} \frac{\lambda_{\rm He\ I\ 2.058\ \mu m}}{\lambda_{\rm Br\gamma}}, \quad \text{for } R_{\rm He^+} < R_{H^+}, \tag{2}$$

and

$$\frac{n_{\rm He}}{n_{\rm H}} = \frac{I_{\rm He\ I\ 2.058\ \mu m}}{I_{\rm Br\gamma}} \frac{\alpha_{\rm Br\gamma}}{\alpha_{\rm He\ I\ 2.058\ \mu m}} \frac{\lambda_{\rm He\ I\ 2.058\ \mu m}}{\lambda_{\rm Br\gamma}}, \quad \text{for } R_{\rm He^+} = R_{H^+}, \tag{3}$$

where I_λ is the flux in the line, $N_{\rm Lyc}$ is the ionizing flux, n is the density, α_B is the total recombination coefficient for all free-bound transitions, α is the total coefficient for all electrons that recombine and make transitions through the specified line, and R is the radius of the ionized volume. The value for $N^{\rm He}_{\rm Lyc}/N^{\rm H}_{\rm Lyc}$ in equation (2) can be taken as a lower limit for $n_{\rm He}/n_{\rm H}$.

Adopting $T_e = 5 \times 10^3$ K and $n_e = 10^2$ cm^{-3} in the gas, we find that $N^{\rm He}_{\rm Lyc}/N^{\rm H}_{\rm Lyc} = 0.14$ according to equation (2), or $n_{\rm He}/n_{\rm H} = 0.15$ according to equation (3), where the recombination coefficients are from Doherty et al. (1994). Our assumed n_e is lower than the value estimated by Lang et al. (1997), $n_e = 640$ cm^{-3}, but such a difference would tend to overestimate the relative He abundance by no more than 10%.

Assuming solar He abundance, such a high value for $N^{\rm He}_{\rm Lyc}/N^{\rm H}_{\rm Lyc}$ suggests $T_{\rm eff} > 35{,}000$ K for the exciting star, regardless of luminosity class (V, III, or I) (Vacca, Garmany, & Shull 1996); furthermore, such a high temperature indicates that $R_{\rm He^+} = R_{\rm H^+}$. Taken together, these results suggest that the star(s) that is exciting the Pistol is hotter than 35,000 K and that the gas in the Pistol is overabundant in helium compared to the solar value, $(n_{\rm He}/n_{\rm H})_\odot = 0.10$; however, we note that, through detailed modeling, a star with $T_{\rm eff}$ between 30,000 and 35,000 K may be able to provide the necessary helium-ionizing flux to account for our measurements (still with an enhanced He abundance).

Lang et al. (1997) also find an enhancement in the helium abundance. They found He92α emission lines over most of the Pistol Nebula, and an average $F_{\rm He\ 92\alpha}/F_{\rm H\ 92\alpha} = 0.14 \pm 0.06$. If the helium and hydrogen ionization zones are coexistent and the dominant form of helium is He$^+$, then this intensity ratio can be taken as the density ratio. While the lower error limit encompasses the solar helium abundance, Lang et al. (1997) did measure a value of 0.19 ± 0.07 in the western region of the nebula, suggesting that the helium content is enhanced in at least part of the Pistol Nebula.

6.6. *Comparison to Previous Work*

Simpson et al. (1997) studied G0.18−0.04 (the Sickle) and the Pistol Nebula in far-infrared forbidden lines. They measured a relatively low value for O^{++}/S^{++} and inferred a high value for $G_{\rm PDR}$. Taken together, they conclude that these values suggest a nearby, but relatively cool, exciting source. Using this, they claim that the Pistol Nebula is ionized by the Pistol Star and that the other Quintuplet

stars are farther from the Pistol Nebula than their projected distances suggest.

We do not directly disagree with their analysis; however, our detection of ionized helium in the Pistol Nebula implies that the exciting star may have $T_{\rm eff} > 35{,}000$ K (see above). This is at odds with the conclusion that only the Pistol Star is ionizing the Pistol Nebula.

Timmermann et al. (1996) also observed the Pistol and the Sickle nebulae in various far-infrared lines. Their nondetection of [O III] 88 μm emission in the Pistol Nebula led them to suggest that the exciting source could not be much hotter than 35,000 K. Again, this is at odds with our observed value of $F_{\rm He\,I\,2.058\,\mu m}/F_{\rm H\,I\,2.166\,\mu m}$.

7. CONCLUSIONS

A combination of photometry, spectroscopy, speckle imaging, and modeling leads to the conclusion that the Pistol Star is extraordinarily luminous. We present two families of models: one predicts $L = 10^{6.6\pm0.2}\,L_\odot$, while the other predicts $L = 10^{7.2\pm0.2}\,L_\odot$. This result, coupled with the relatively low temperature, $T_{\rm eff} \gtrsim 10^{4.15\pm0.01}$ K, implies that the star exceeds the Humphreys-Davidson limit. Our previous suggestion that the Pistol Star is a luminous blue variable is supported by the star's position in the H-R diagram and the detection of variability in the Brackett-γ line. Further monitoring will be necessary to establish photometric variability.

Our stellar evolution calculations, which suggest an initial mass and age of 200–250 $M_\odot$ and 1.7–2.1 Myr (see § 5.2), confirm that it may currently be in an unstable evolutionary phase (Stothers & Chin 1997).

In addition, we argue that the surrounding Pistol Nebula (G0.15 − 0.05) is photoionized circumstellar ejecta from the star. This claim is supported by (1) the common velocity of the star and the nebula, (2) the similarity in nebular parameters of the Pistol Nebula and LBVN, (3) the velocity profiles in the Pistol Nebula , (4) the morphology of the Pistol Nebula, (5) the likelihood that a massive star like the Pistol Star might have recently ejected material, and (6) the agreement between the surface helium abundance predicted by our stellar evolution models, the observed photospheric helium abundance of the Pistol Star, and the derived helium abundance of the nebula. The star might not be currently hot enough to ionize the Pistol gas, but it might have recently been hot enough so that the gas is still recombining. Alternatively, other nearby hot stars might be ionizing the Pistol Nebula.

We acknowledge useful discussions with Eric E. Becklin, E. L. Wright, Roger Ulrich, Cornelia Lang, Murray D. Silverstone, Rolf Kudritzki, and Daniel J. Lennon. B. L. Klein & C. McCabe assisted in obtaining and reducing the speckle-imaging data. We would like to thank John Hillier for kindly providing us with his atmospheric code. Finally, we thank the referee, who provided a very thorough critique of the paper, giving many useful comments and suggestions. F. N. acknowledges a grant of the DARA under WE2-50 OR 9413 6. N. L. has been supported by the Deutsche Forschungsgemeinschft through grant La 587/15-1. Some of the observations were obtained as part of the UKIRT Service Programme. UKIRT is operated by the Joint Astronomy Centre on behalf of the United Kingdom Particle Physics and Astronomy Research Council. Some of the data presented herein were obtained at the W. M. Keck Observatory, which is operated as a scientific partnership among the California Institute of Technology, the University of California, and the National Aeronautics and Space Administration. The Observatory was made possible by the generous financial support of the W. M. Keck Foundation.

REFERENCES

Allen, D. A., Jones, T. J., & Hyland, A. R. 1985, ApJ, 291, 280
Altamore, A., Maillard, J.-P., & Viotti, R. 1994, A&A, 292, 208
Bashkin, S., & Stoner, J. O., Jr. 1975, Atomic Energy Levels and Grotrian Diagrams, Vol. 1 (Amsterdam: North-Holland)
Becklin, E. E., Matthews, K., Neugebauer, G., & Willner, P. 1978, ApJ, 220, 831
Blum, R. D., DePoy, D. L., & Sellgren, K. 1995, ApJ, 441, 603
Cardelli, J. A., Clayton, G. C., & Mathis, J. S. 1989, ApJ, 345, 245
Carr, J. S., Sellgren, K., & Balachandran, S. 1996, in ASP Conf. Proc. 102, The Galactic Center, 4th ESO/CTIO Workshop, ed. R. Gredel (San Francisco: ASP), 212
Chiosi, C., & Maeder, A. 1986, ARA&A, 24, 329
Conti, P. S. 1984, in IAU Symp. 105, Observational Tests of Stellar Evolution Theory, ed. A. Maeder & A. Renzini (Dordrecht: Reidel), 233
Cotera, A. S., Erickson, E. F., Colgan, S. W. J., Simpson, J. P., Allen, D. A., & Burton, M. G. 1996, ApJ, 461, 750
Crowther, P. A., Hillier, D. J., & Smith, L. J. 1995, A&A, 293, 172
Damineli, A., Conti, P. S., & Lopes, D. F. 1997, NewA, 2, 107
de Jager, C., Niheuvenhuijzen, H., & van der Hucht, K. A. 1988, A&A, 72, 259
DePoy, D. L., & Shields, J. C. 1994, ApJ, 422, 187
Doherty, R. M., Puxley, P., Doyon, R., & Brand, P. W. J. L. 1994, MNRAS, 266, 497
Figer, D. F. 1995, Ph.D. thesis, Univ. California, Los Angeles
Figer, D. F., McLean, I. S., & Morris, M. 1995, ApJ, 447, L29 (FMM95)
———. 1998, in preparation
Figer, D. F., Morris, M., & McLean, I. S. 1996, in ASP Conf. Ser. 102, The Galactic Center, 4th ESO/CTIO Workshop, ed. R. Gredel (San Francisco: ASP), 263 (FMM96)
Fliegner, J., & Langer, N. 1995, in IAU Symp. 163, Wolf-Rayet Stars: Binaries, Colliding Winds, Evolution, ed. K. A. van der Hucht & P. M. Williams (Dordrecht: Kluwer), 326
Fliegner, J., Langer, N., & Venn, K. 1996, A&A, 308, L13
Garcia, J. D., & Mack, J. E. 1965, J. Opt. Soc. Amer., 55, 654
Garmany, C. D. 1988, in O Stars and Wolf-Rayet Stars, NASA SP 497, ed. P. S. Conti, & A. B. Underhill (Washington, DC: US GPO), 160
Ghez, A. M., Klein, B. L., Morris, M., & Becklin, E. E. 1998, ApJ, in press
Glass, I. S., Catchpole, R. M., & Whitelock, P. A. 1987, MNRAS, 227, 373
Glass, I. S., Moneti, A., & Moorwood, A. F. M. 1990, MNRAS, 242, 55P
Hamann, F., DePoy, D. L., Johansson, S., & Elias, J. 1994, ApJ, 422, 626
Heger, A., & Langer, N. 1996, A&A, 315, 421
Hillier, D. J. 1987, ApJS, 63, 947
———. 1990, A&A, 231, 116
Hoffman, M., Stift, M. M., & Moffat, A. F. J. 1978, PASP, 90, 101
Hu, J. Y., de Winter, D., The, P. S., & Perez, M. R. 1990, A&A, 227, L17
Humphreys, R. M., & Davidson, K. 1979, ApJ, 232, 409
———. 1994, PASP, 106, 1025
Israelian, G., De Groot, M., Parker, J. W., & Sterken, C. 1996, MNRAS, 283, 119
Johansson, S. 1978, Phys. Scr., 18, 217
Kaplan, S. A., & Pikelner, S. B. 1970, The Interstellar Medium (Cambridge: Harvard Univ. Press), 50
Koenigsberger, G., Auer, L. H., & Guinan, E. 1997, ApJ, 496, 934
Koornneef, J. 1983, A&A, 128, 84
Kudritzki, R.-P., Lennon, D. J., Haser, S. M., Puls, J., Pauldrach, A. W. A., Venn, K., & Voels, S. A. 1996, in Science with the Hubble Space Telescope, Vol. II, ed. P. Benvenuti, F. D. Machetto, & E. J. Schreier (Baltimore: STScI), 135
Kudritzki, R.-P., Pauldrach, A., Puls, J., & Abbott, D. C. 1989, A&A, 219, 205
Landini, M., Natta, A., Salinari, P., Oliva, E., & Moorwood, A. F. M. 1984, A&A, 134, 284
Lang, C. C., Goss, W. M., & Wood, D. O. S. 1997, ApJ, 474, 275
Langer, N. 1992, A&A, 265, L17
———. 1997, in ASP Conf. Proc. 120, Luminous Blue Variables: Massive Stars in Transition, ed. A. Nota & H. J. G. L. M. Lamers (San Francisco: ASP), 83
———. 1998, A&A, 329, 551
Langer, N., Hamann, W.-R., Lennon, M., Najarro, F., Puls, J., & Pauldrach, A. 1994, A&A, 290, 819
Le Bertre, T., Epchtein, N., Gouiffes, C., Heydari-Malayeri, M., & Perrier, C. 1989, MNRAS, 225, 417

Leitherer, C. 1997, in ASP Conf. Proc. 120, Luminous Blue Variables: Massive Stars in Transition, eds. A. Nota & H. J. G. L. M. Lamers (San Francisco: ASP), 58
Lutz, D., et al. 1996, A&A, 315, L269
Maeder, A. 1987, A&A, 178, 159
Maeder, A., & Meynet, G. 1994, A&A, 287, 803
Marston, A. P. 1995, AJ, 109, 2257
Massey, P., & Hunter, D. A. 1998, ApJ, 493, 180
Matthews, K., Ghez, A. M., Weinberger, A. J., & Neugebauer, G. 1996, PASP, 108, 615
Matthews, K., & Soifer, B. T. 1994, in Infrared Astronomy with Arrays: the Next Generation, ed. I. S. McLean (Dordrecht: Kluwer), 239
McCarthy, J. K., Kudritzki, R.-P., Lennon, D. J., Venn, K. A., & Puls, J. 1997, ApJ, 482, 757
McGregor, P. J., Hyland, A. R., & Hillier, D. J. 1988, ApJ, 324, 1071
McLean, I. S., et al. 1993, Proc. SPIE, 1946, 513
———. 1994, Proc. SPIE, 2198, 457
Meaburn, J., Lopez, J. A., Barlow, M. J., & Drew, J. E. 1996, MNRAS, 283, L69
Meynet, G. 1995, A&A, 298, 767
———. 1998, in ASP Conf. Proc., Proc. 2nd Boulder-Munich Workshop, ed. I. Howarth (San Francisco: ASP), in press
Meynet, G., Maeder, A., Schaller, G., Schaerer, D., & Charbonnel, C. 1994, A&AS, 103, 97
Moffat, A. F. J. 1983, A&A, 124, 273
Moneti, A., Glass, I. S., & Moorwood, A. F. M. 1994, MNRAS, 268, 194
Morris, P. W., Eenens, P. R. J., Hanson, M. M., Conti, P. S., & Blum, R. D. 1996, ApJ, 470, 597
Nagata, T., Hyland, A. R., Straw, S. M., Sato, S., & Kawara, K. 1993, ApJ, 406, 501
Nagata, T., Woodward, C. E., Shure, M., Pipher, J. L., & Okuda, H. 1990, ApJ, 351, 83
Najarro, F. 1995, Ph.D. thesis, Ludwig-Maximilian Univ.
Najarro, F., Krabbe, A., Genzel, R., Lutz, D., Kudritzki, R. P., & Hillier, D. J. 1997, A&A, 325, 700
Nota, A., Livio, M., Clampin, M., & Schulte-Ladbeck, R. 1995, ApJ, 448, 788
Okuda, H., et al. 1990, ApJ, 351, 89
Panagia, N., Gilmozzi, R., Macchetto, F., Adorf, H.-M., & Kirshner, R. P. 1991, ApJ, 380, L23
Pasquali, A. 1997, in ASP Conf. Proc. 120, Luminous Blue Variables: Massive Stars in Transition, ed. A. Nota & H. J. G. L. M. Lamers (San Francisco: ASP), 13
Pauldrach, A. W. A., Kudritzki, R. P., Puls, J., Butler, K., & Hunsinger, J. 1994, A&A, 283, 525
Puls, J., et al. 1996, A&A, 305, 171
Reader, J., & Corliss, C. H. 1980, Wavelengths and Transition Probabilities for Atoms and Atomic Ions, Part I. Wavelengths (Washington, DC: NBS)
Reid, M. J. 1993, ARA&A, 31, 345
Rieke, G. H., Rieke, M. J., & Paul, A. E. 1989, ApJ, 336, 752 (RRP)
Schaller, G., Schaerer, D., Meynet, G., & Maeder, A. 1992, A&AS, 96, 269
Shields, J. C., & Ferland, G. J. 1994, ApJ, 430, 236
Simpson, J. P., Colgan, S. W. J., Cotera, A. S., Erickson, E. F., Haas, M. R., Morris, M., & Rubin, R. H. 1997, ApJ, 487, 689
Smith, L. J., Crowther, P. A., & Prinja, R. K. 1994, A&A, 281, 833
Stothers, R. B., & Chin, C.-W. 1997, ApJ, 489, 319
Tamblyn, P., Rieke, G. H., Hanson, M. M., Close, L. M., McCarthy, D. W., Jr., & Rieke, M. J. 1996, ApJ, 456, 206
Theodossiou, E., & Danezis, E. 1991, Ap&SS, 183, 91
Timmermann, R., Genzel, R., Poglitsch, A., Lutz, D., Madden, S. C., Nikola, T., Geis, N., & Townes, C. H. 1996, ApJ, 466, 242
Tokunaga, A. 1986, IRTF Photometry Manual, University of Hawaii, internal report
Vacca, W. D., Garmany, C. D., & Shull, J. M. 1996, ApJ, 460, 914
Wainscoat, R. J., & Cowie, L. L. 1992, AJ, 103, 332
Walborn, N. R., & Blades, J. C. 1997, ApJS, 112, 457
Walker, A. R., & O'Donoghue, D. E. 1984, Astron. Express, 1, 45
Weigelt, G. 1981, in Scientific Importance of High Angular Resolution at Infrared and Optical Wavelengths, ed. M. H. Ulrich & K. Kjaer (Munich: ESO), 95
Wilson, R. E. 1953, in General Catalogue of Stellar Radial Velocities (Washington, DC: Carnegie Institution of Washington), 213
Yusef-Zadeh, F., & Morris, M. 1987, AJ, 94, 1178
Yusef-Zadeh, F., Morris, M., & van Gorkom, J. H. 1989, in IAU Symp. 136, The Center of the Galaxy, ed. M. Morris (Dordrecht: Kluwer), 275
Zickgraf, F.-J., Kovacs, J., Wolf, B., Stahl, O., Kaufer, A., & Appenzeller, I. 1996, A&A, 309, 505
Zickgraf, F.-J., Wolf, B., Stahl, O., Leitherer, C., & Appenzeller, I. 1986, A&A, 163, 119